Available online at www.sciencedirect.com
SCIENCE DIRECT
Remote Sensing of Environment 102 (2006) 33–51
Remote Sensing of Environment
www.elsevier.com/locate/rse

Spatial scaling of evapotranspiration as affected by heterogeneities in vegetation, topography, and soil texture

Mustapha El Maayar *, Jing M. Chen

Department of Geography, University of Toronto, 100, St. Georges Street, Toronto, Ontario, Canada M5S 3G3

Received 18 May 2005; received in revised form 25 January 2006; accepted 26 January 2006

Abstract

To date, simulating land surface hydrological processes over large areas at spatial resolutions higher than 1 km remains technically unfeasible, because of limitations of data availability and computational resources. Several studies have demonstrated, however, that gridding the land surface into coarse homogeneous pixels may cause important biases on ecosystem model estimations of water budget components at local, regional and global scales. These biases result from the overlook of sub-pixel variability of land surface characteristics. This study suggests a simple algorithm that uses sub-pixel information on the spatial variability of vegetation and soil cover, and surface topography to correct evapotranspiration (ET) estimates, made at coarse spatial resolutions where the land surface is considered as homogeneous within each pixel. The algorithm operates in such a way that the ET rates as obtained from calculations made at coarse spatial resolutions are multiplied by separate simple functions that attempt to reproduce the effects of sub-pixel variability of land cover, leaf area index, soil texture, and topography on ET. Its application to a remote sensing process-based model estimates made at a 1-km resolution over a watershed located in the southern part of the Canadian boreal forest improved estimates of average ET as well as its temporal and spatial variability.

Keywords: Evapotranspiration; Sub-pixel heterogeneity; Land cover; Topography; Soil texture; Spatial scaling

1. Introduction

Spatial scaling of land surface processes, such as land surface–atmosphere exchanges of water and carbon, has been recognized as one of the most difficult and challenging issues in environmental sciences (Bonan et al., 2002; Chen, 1999; Jarvis, 1995; Kimball et al., 1999). Scaling refers to the use of information available at one scale to derive processes that occur at a higher/finer (down-scale) or a lower/coarser (up-scale) scale. Downscaling, on one hand, is generally required for the use of available information at a given resolution to a system where some processes operate at a higher resolution. For instance, some scientists develop algorithms to downscale meteorological data obtained from climate model simulations made at coarse spatial resolutions (e.g., 5 × 5°), for their use in ecosystem studies where analyses at higher spatial resolutions are desired (e.g., Price et al., 2000). Up-scaling, on the other hand, is required to expand knowledge from a fine to a coarser resolution. Scaling of photosynthesis from leaf to canopy in ecosystem models is one of the most widely known up-scaling examples.

The up-scaling of ecological processes requires necessarily a simplification of the landscape complexity. Such a simplification is a critical issue in land surface modeling as ecosystem model simulations depend closely upon the representation of land surface heterogeneity. In many of these models for example, vegetation at each grid cell is represented by the dominant vegetation type in that cell. This yields some situations where the land cover of a grid cell might be represented by a land cover type that cover less than half of the total area of the grid cell, which may inevitably cause model predictions to be significantly biased (e.g., Chen, 1999; Gower et al., 2001; Rastetter et al., 1992, 2003; Strayer et al., 2003). Several studies have illustrated for example that the overlook or the oversimplification of land surface complexity may cause ecosystem models simulations of surface hydrology to be

* Corresponding author. Tel.: +1 416 946 3058; fax: +1 416 946 3886.
E-mail address: elmaayarm@geog.utoronto.ca (M. El Maayar).

0034-4257/$ - see front matter © 2006 Elsevier Inc. All rights reserved.
doi:10.1016/j.rse.2006.01.017

considerably biased (Arora et al., 2001; Band et al., 1993; Grant, 2004; Haddeland et al., 2002; Kimball et al., 1999; Mackay et al., 2002; Mitchell et al., 2005).

To partially reduce the biases of ecosystem model simulations, several approaches had been proposed during the last two decades to improve the representation of land surface heterogeneity in these models. This includes the so-called explicit, statistical, and contributing area approaches. Explicit approaches are those where each land pixel is divided into multiple sub-pixels or patches to account for surface heterogeneity in model calculations (e.g., Avissar & Pielke, 1989; Koster & Suarez, 1992; Seth et al., 1994; Verseghy et al., 1993; Walko et al., 2000). Statistical approaches are those where probability distribution functions are used to capture the variability of surface properties/parameters within each grid cell [e.g., soil physical hydrological properties] (e.g., Bonan et al., 1993; Entekhabi and Eagleson, 1989; Wetzel and Chang, 1988; Wood et al., 1992). In both explicit and statistical approaches, the surface energy budget is solved for every sub-grid area to finally yield a weighted solution for the entire grid cell, which might be very costly in terms of computational time. The contributing area method suggests on other hand that existing sub-grid land surface information of soil properties and surface topography may be used to calibrate model parameters (e.g., Band et al., 1991; Douville, 1998; Dümenil & Todini, 1992; Famiglietti & Wood, 1994; Pellenq et al., 2003). Additionally to the three above approaches, Boone and Wetzel (1998) suggested an approach where each grid cell is considered as a juxtaposition of parallel soil columns. Soil hydrological parameters of each column were determined thereafter using statistical relationships (regressions) between the hydrological parameters and the soil texture of these columns. Using their methodology for climate model simulations, Boone and Wetzel (1998) found that accounting for soil texture variability within each pixel reduced global ET by 17% and increased total runoff by 48% and soil wetness by 19%, compared to the case in which a homogenous soil texture was assigned to the entire soil column.

Naturally, each of the three above approaches has limitations and advantages. In practice, the adoption of one of them instead of the others to represent "effective" surface heterogeneity must be dictated by the particular purpose of use. Thus, because there is no unique way to represent effectively surface heterogeneity (Strayer et al., 2003), Simic et al. (2004) proposed a methodology where ecosystem model simulations made at any spatial resolution may be corrected if sub-grid information of land heterogeneity exists. Indeed, rather than attempting to adequately represent surface heterogeneity within the land model, Simic et al. (2004) suggest the use of sub-grid information on surface heterogeneity to directly correct model estimates of net primary production (NPP). To map NPP at a 30-m resolution, Simic et al. (2004) adjusted remote sensing based ecosystem model estimates made at a 1-km resolution by multiplying the simulated NPP at 1-km resolution by a function that correct for land cover and LAI variability within each of the 1-km pixels. Simic et al.'s methodology was in fact built on the logic that while it is difficult to perform calculations of NPP, or any other variable, for large regions such as Canada at any resolution higher than 1 km because of limitations inherent to data availability and computational resources, it is nevertheless possible to exploit sub-1-km pixel information whenever they exist to correct calculations of the variable in question, made at resolutions that may be lower than or equal to 1 km. The emergence of that methodology to down-scale model estimations made at coarse spatial resolutions had been encouraged by recent progress in mapping land cover characteristics using remote sensing observations. In fact, while land cover features could be mapped over large regions using satellite observations at a 1-km resolution, some emerging classification techniques demonstrated an acceptable accuracy in using these 1 km maps to extract the fraction of each land cover type present within each pixel (e.g., Canters et al., 2002). At high resolutions in practice, it is always much easier to map land cover types and vegetation density than to model the complex surface process at the same resolutions.

Accurate estimates of water budget components at regional, continental, and global scales are critical for the establishment of adequate land resources management strategies. Accurate estimates of ET are, for example, important for the derivation of soil moisture and runoff over large basins, and the prediction of large river discharges (e.g., Nijssen, Lettenmaier et al., 1997). At smaller scales, Liu et al. (2003) reported that adequate estimates of regional ET should enhance the reliability of runoff estimations for ungauged watersheds in support of hydroelectric power generation. Investigating and reducing sources of uncertainties that are associated with model predictions of ET are therefore crucial issues. The objective of this study is to develop a simple algorithm that could be used to correct and down-scale ecosystem model estimates of ET. The philosophy of our algorithm and the one developed by Simic et al. (2004) are similar. However, while Simic et al.'s algorithm includes one single corrective component where land cover and leaf are index (LAI) corrections are dependants, our algorithm includes four corrective components where each one of these components is completely independent from the three others. The four components of our algorithm are: land cover, LAI, soil texture, and topography. In particular, the consideration of topography in downscaling requires the use of a hydrological model that is capable of simulating the lateral ground water flow influencing the spatial ET distribution pattern, and results from this work can be, therefore, potentially applicable not only to flat areas but also to areas with a complex topography.

2. Methodology

2.1. Model used

We used the distributed hydrology-vegetation model (TerrainLab) described in details in Chen et al. (2005). TerrainLab borrows its basic structure from Wigmosta et al.'s (1994) model, but with several modifications to maximize its use for remote sensing applications. It operates at a daily time-step, and incorporates the effects of land topography on the hydrological cycle, by simulating the water flow between neighboring pixels. For that purpose, a moving window of 3×3 pixels is used to

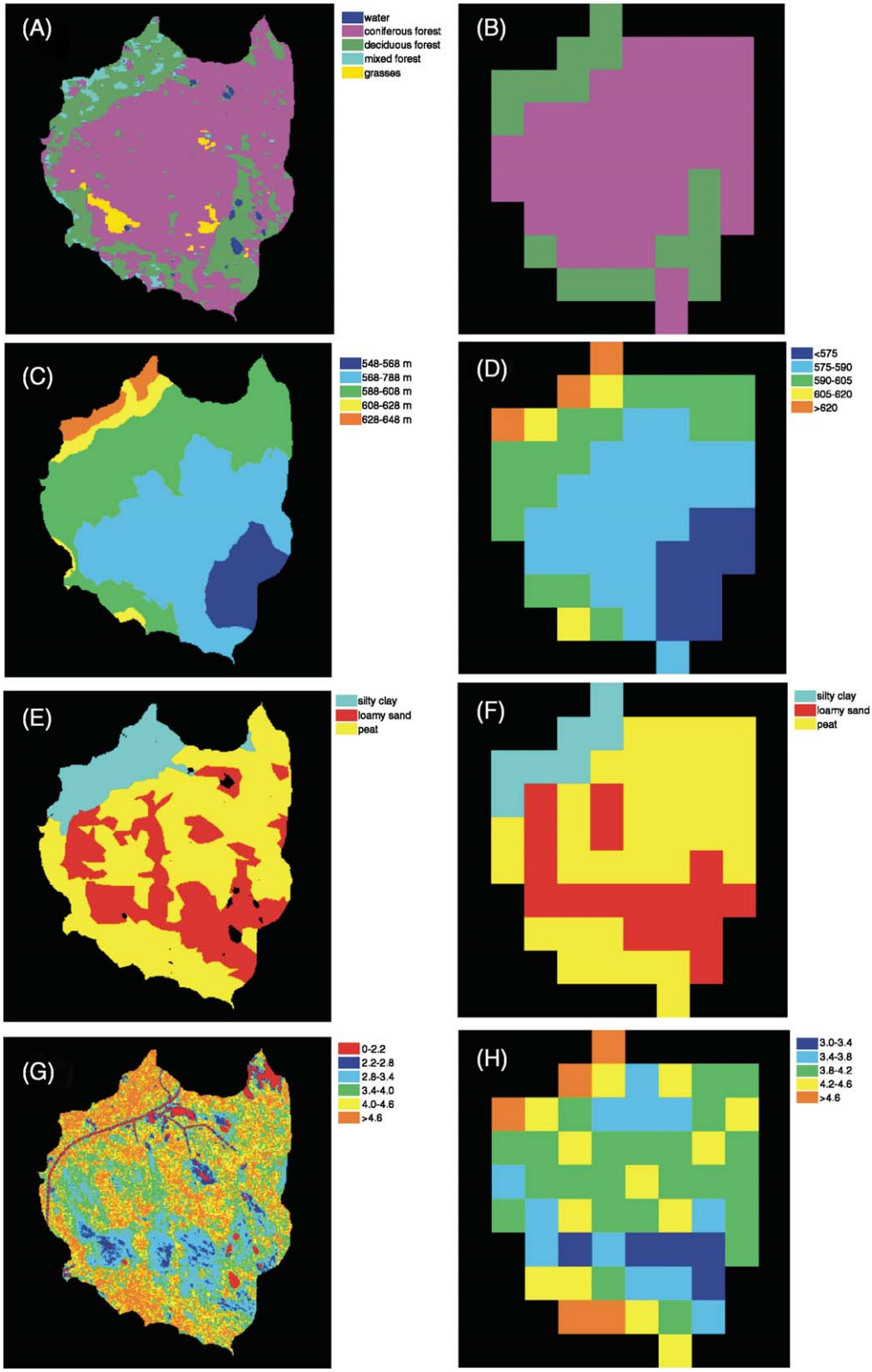

Plate 1. Watershed characteristics at 30-m and 1-km resolutions: (A) Land cover at 30-m resolution; (B) Land cover at 1-km resolution; (C) Elevation at 30-m resolution; (D) Elevation at 1-km resolution; (E) Soil type at 30-m resolution; (F) Soil type at 1-km resolution; (G) Leaf area index at 30-m resolution; (H) Leaf area index at 1-km resolution.

estimate the lateral saturated base flow according to the water table as affected by surface topography and soil drainage. The model subdivides vegetation into three layers, namely overstory, understory and litter-moss. The soil is divided into saturated and unsaturated zones; wherein the depth varies accordingly with water table fluctuations. Following the approach of Jarvis (1976), the stomatal conductance is calculated as the product of its potential maximum and a set of empirical functions to account for leaf's stomatal response to the ambient conditions including air temperature, photosynthetic photo flux density, air vapour pressure deficit, and soil water content. Moreover, the model assumes that plant roots can extract water either from unsaturated or/and saturated zones. The root vertical distribution is modeled according to Jackson et al. (1996), where a simple asymptotic equation is used to represent the vertical root profile. The model does include a routine that simulates the effect of topography on the surface radiation budget by considering the geometry between the solar beam and the normal to the slope according to Campbell and Norman (1998).

Required meteorological inputs include mean air temperature, precipitation, solar radiation, and relative humidity. Required soil data include soil depth, and soil texture, from which associated soil hydrological properties including porosity, saturated hydraulic conductivity, wilting point, and saturated suction are estimated. To account for the influence of topographical variations on the water budget components, a digital terrain model (DEM) is also required, from which slope and aspect are calculated. Needed vegetation information include land cover type and LAI.

The performance of the model and its different components is detailed in Appendix A.

2.2. Site description and data preparation

The study area is a watershed located in the Southern Study Area (SSA) of the Boreal Ecosystem-Atmosphere Study (BOREAS). The hydrological modeling domain encompasses the old black spruce (SSA-OBS) stand, about 30 km northeast from Candle Lake, Saskatchewan (53.99°N, 105.12°W), Canada. Monthly temperature varies from −16.9 °C in January to about 16.7 °C in July, and the annual precipitation is approximately 400 mm. The soil originates predominantly from Glacial Lake Agassiz sediments and consists of sand, clay and organic matter. The topography has low relief and poor drainage (Nakane et al., 1997). The site for the present study comprises 360 by 360 pixels at 30 m resolution. The watershed studied here is in a typical Canadian shield landscape with gentle and moderate topographical variations on top of a shallow bedrock (Branfireun & Roulet, 1998). In the landscape, slopes with shallow overburden may be decoupled with receiving streams in dry seasons (Devito et al., 1996). This particular watershed drains to a small lake through saturated subsurface flows and ephemeral streams.

The forests within the modeling domain (Plate 1A) are typical of southern boreal forests, consisting primarily of black spruce (*Picea mariana* (Mill.) BSP) with small patches of jack pine (<2% in tree count) (*Pinus banksiana* Lamb.), and other tree species (<3%) including tamarack (*Larix laricina* [Du Roi] K. Koch) and willow (*Salix* spp.) (Gower et al., 1997). The basal areas of the stands are 30 m^2 ha^{-1} (Jarvis et al., 1997) and the average leaf area index (LAI) at the OBS site is 4.5 (Chen et al., 1997). The understory is composed of grasses of variable densities and sparse shrubs above an extensive moss ground cover. The growing season is normally limited to the summer

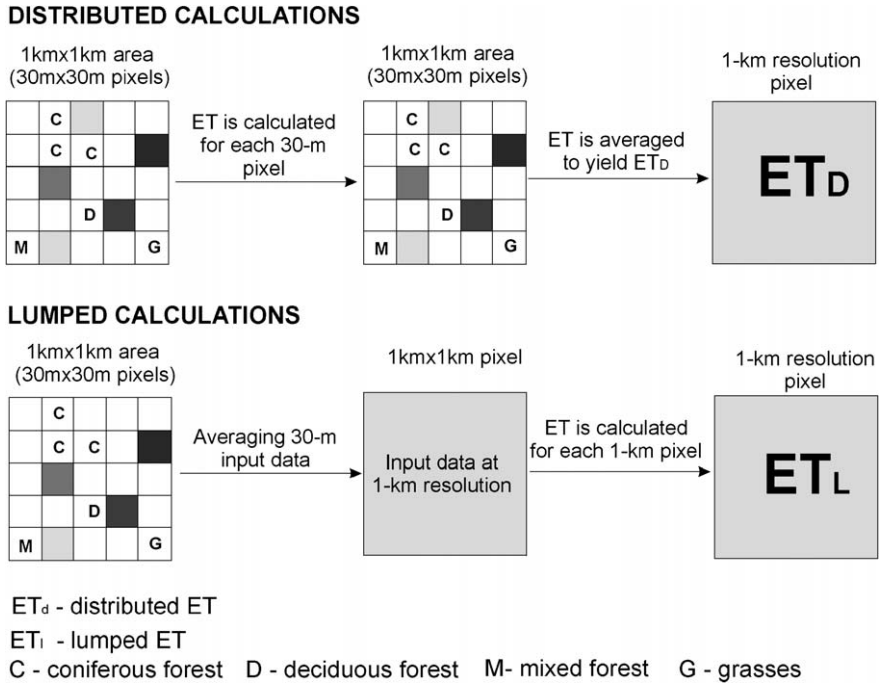

Fig. 1. Scheme of the procedures that were followed in the lumped and distributed calculations of ET.

months between May and September when the daily temperature is above 5 °C. Our study is, henceforth, limited to the growing season of year 1994 (day number of the year from 150 through 250).

The procedures used to preprocess various spatial input datasets are explained in Appendix B.

2.3. Simulation procedures

Two simulations were made to analyze the bias in coarse resolution ET estimates. The first simulation was made at 30-m resolution using input datasets at the same resolution (see Section 2.2), while the second simulation was made at a 1-km resolution after resampling the 30-m resolution datasets to a 1-km resolution (see next paragraph). Obtained ET from the simulation made at the 30-m resolution is referred to as distributed ET, or ET_d; while obtained ET from the simulation made at the 1-km resolution is hereafter referred to as lumped ET, or ET_l. For comparison with ET_l, ET_d was resampled to 1-km resolution as illustrated in Fig. 1. Each model run had its own spin-up. In fact, the 30-m run spin-ups were not aggregated to initialize the lumped 1-km runs.

To perform the 1-km simulation, input data available at the 30-m resolution were averaged (resampled) to obtain input datasets at 1-km resolution (Fig. 1). As usual, however, land cover and soil texture types of each 1-km pixel were assumed to be the dominant type in the aggregated 30-m pixels. Therefore, a distributed 1-km pixel contains a maximum of 1089 (33×33) heterogeneous 30-m pixels, while a lumped 1-km pixel contains unique homogeneous vegetation and soil types. Our choice of these two resolutions was motivated by the following considerations: (i) the 1-km pixel size corresponds to the resolution at which land cover information from a satellite is usually available at regional and global scales; (ii) the 30-m pixel size represents the resolution beyond which it becomes difficult to represent adequately the mosaics of soil and vegetation found in the southern Canadian boreal forest (Bonan & Shugart, 1989), where our watershed is located.

Separate analyses of the effects of the variability of land cover, soil texture and surface topography within the 1-km pixels on the ET_d/ET_l ratio were used to develop our algorithm.

3. Results

3.1. Aggregation effects on the watershed's characteristics

At the 30-m resolution, five land cover classes are distinguished (Plate 1A). They include coniferous forest (CF), broadleaf deciduous forest (DF), mixed (conifer-broadleaf deciduous) forest (MF), grasses (Gr), and small patches of open water (OW). CF is the dominant land cover type as it occupies nearly 66% of the total watershed area, followed by DF (28%), MF (3%) and Gr (2%), respectively. After aggregating these land cover types to 1-km resolution, MF and Gr classes disappeared, the proportion of CF became 72%, and the proportion of DF (28%) remained unchanged (Plate 1B). Results of this aggregation are consistent with comparisons of Landsat TM (30-m resolution) and NOAA-AVHRR (1-km resolution) land cover maps of the BOREAS-southern study area (Hall et al., 1997; Steyaert et al., 1997).

At 30-m resolution, the loamy-sand, silty-clay and peat are the three soil textural classes found in the watershed (Plate 1C). As it may be expected, loamy-sand soil that occupies about 58% of the total soil surface is generally found in regions where CF dominates, while silty-clay soil that occupies 13% is generally found in regions where DF dominates (Plate 1A and C). Peat soil occupies about 29%, and is found in regions that contain either CF or DF. After the aggregation to 1-km resolution (Plate 1D), the proportion of the loamy-sand, silty-clay and peat soils became only slightly different from those found at 30-m resolution as they established to 59%, 12% and 29%, respectively.

The elevation within the watershed varies between a minimum of 549 m and a maximum of 648 m at the 30-m resolution, and between a minimum of 552 m and a maximum of 632 m at 1-km resolution. Logically, the elevation range (maximum–minimum) is larger at 30 m (elevrange = 99 m) than at 1 km (elevrange = 80 m) resolution (Plate 1E and F). Minimum and maximum LAI are 1.7 and 5.4 at the 30 m resolution, and are 3 and 4.7 at the 1-km resolution, respectively (Plate 1G and H).

It is worth noting that the relatively small change in the proportions of CF and DF land covers and soil types that resulted from the aggregation from 30 m to 1 km, hide the fact that some coarse pixels (1 km) may be dominated by some land cover and soil types, while in reality, they encompass substantial proportions of other land cover and soil types. For instance, the 1 km lumped pixel located in line7-pixel3 (Plate 1B), is dominated by CF. In that pixel in reality, CF forms only 39% of the total land cover versus 35% for DF, and 26% for Gr. Similarly, loamy-sand is the dominant soil texture (60%) in the lumped pixel having the coordinates line3-pixel5 (Plate 1D), while in reality, silty-clay and peat soils are present in proportions of 36% and 4%, respectively.

3.2. Effects of aggregating input data on ET estimates

At the 30 m resolution, the average simulated watershed's ET (ET_d) over the entire period of the study (days of year 150–250) varied between a minimum of 0.50 and a maximum of 3.74 mm/day, and averaged to 1.89 mm/day (Table 1 and Fig. 2A–C). For pixels dominated by conifer and deciduous forests, ET averaged to 1.66 and 2.54 mm/day, respectively. For the entire watershed area, lumped calculations yielded an average ET (ET_l) that is only 4% higher than ET_d, but average ET_l was 8% lower and 24% larger than ET_d for CF and DF, respectively (Table 1). Using the BIOME-BGC model and data from the same region (BOREAS southern study area) to examine the effect of spatial heterogeneity on average estimated ET, Kimball et al. (1999) found fairly comparable results.

95% of this watershed area is either covered by CF or DF. Because CF generally have a lower ET than DF and MF under similar climatic and edaphic conditions, we may anticipate that a lumped coniferous pixel would yield a lower average ET than

Table 1
Statistics of distributed and lumped ET

	Distributed ET			Lumped ET before correction			Lumped ET after correction		
	Coniferous pixels	Deciduous pixels	All pixels	Coniferous pixels	Deciduous pixels	All pixels	Coniferous pixels	Deciduous pixels	All pixels
Average	1.66	2.54	1.89	1.53	3.16	1.98	1.75	2.33	1.91
MBE	na	na	na	−0.14	0.62	0.08	0.09	−0.21	0.02
Minimum	0.48	0.55	0.50	0.46	0.70	0.55	0.54	0.50	0.55
Maximum	3.29	5.00	3.74	2.98	5.84	3.77	3.45	4.33	3.69
Range	2.81	4.45	3.24	2.52	5.14	3.22	2.91	3.83	3.14

Shown are averaged values of ET obtained over all coniferous and deciduous pixels, and all pixels of the watershed; over the entire period of study (days of year from 150 to 250). MBE refers to the mean bias error. All values are expressed in mm/day.

the corresponding distributed pixel covered by both CF and DF. This is because only CF is considered in lumped calculations, while both CF and DF are considered in distributed calculations. Conversely, we may anticipate that a lumped deciduous pixel would yield a higher average ET than the corresponding distributed pixel covered by both CF and DF land cover types. Obtained results shown in Table 1 and Fig. 2A,B confirmed these anticipations as lumping negatively biased average ET of CF pixels (−8%) and positively biased ET of DF pixels (+24%). As a direct consequence, the negative bias of CF's ET_l and the positive bias of DF's ET_l cancelled each other and yielded an overall low positive bias (4%) for the entire watershed's average

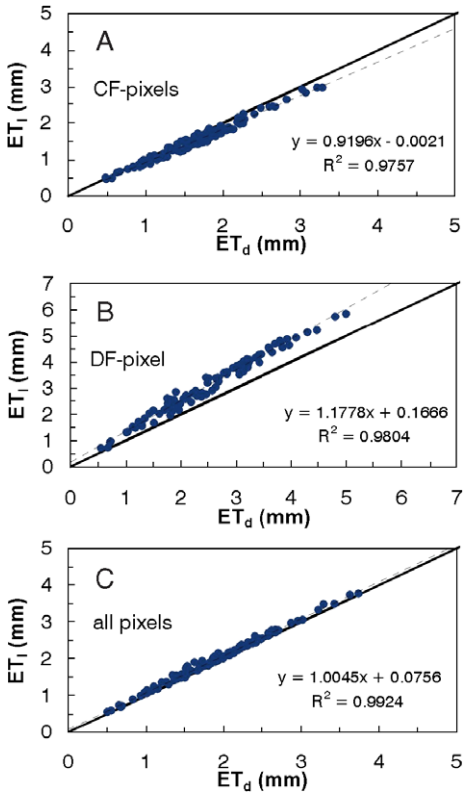

Fig. 2. Regression between lumped (ET_l) and distributed (ET_d) daily values of ET (day of year 150 through day of year 250), before correction. Each point represents obtained average ET on a given day, over: (A) all pixels dominated by the coniferous forest (CF pixels); (B) all pixels dominated by the deciduous forest (DF pixels); (C) all pixels of the watershed.

ET_l. Moreover, a more exhaustive exploration of the results indicates that the inherent bias to lumping could be much more substantial for single pixels regarding daily ET rates (Fig. 3A–C). For instance, the correlation (r^2, and also the slope and the intercept) between daily ET_d and ET_l values obtained for each pixel shown in Fig. 3A–C is much lower than r^2 of the watershed's average values of ET_d and ET_l (Fig. 2A–C). This suggests that lumping induces a larger bias on the spatial distribution than the temporal distribution of ET.

3.3. Correction of lumped ET: description and application of the corrective algorithm

The starting point for our algorithm is based on the assumption that ET_d and ET_l represent the correct and the biased ET, respectively. This is because the surface heterogeneity is preserved in the distributed calculations, while it is not in the lumped calculations (Fig. 1). Therefore, the objective is to derive a multiplicative factor that may be used to correct ET_l values, and subsequently reduces the difference between ET_d and ET_l. Thus, we expressed the relationship between ET_d and ET_l merely as:

$$ET_d = ET_l.R \quad (1)$$

where R represents the multiplicative factor that is needed for the correction of ET_l.

ET_l is biased because only the dominant land cover and soil texture in coarse (1 km) pixels are used in its calculation, and because input data of LAI and topography represent only average conditions within each coarse pixel. It is known, however, that the responses of ET to LAI and topographical variations are non-linear (e.g., Campbell & Norman, 1998; Kenward et al., 2000). In fact, because of the non-linear ET–LAI relationship, ET rate calculated as the average of ETs of two adjacent pixels having different LAIs (distributed calculation) will most likely be different than the ET rate calculated using the average LAI of the two pixels (lumped calculation). Similarly, under similar soil and vegetation conditions, ET of a pixel located on an abrupt slope is likely (a-priori) to be lower than ET of a pixel located in a flat region, even though the two pixels have similar average elevations. This is because the fraction of precipitation that may be partitioned into runoff could be much larger over bumpy than over flat surfaces,

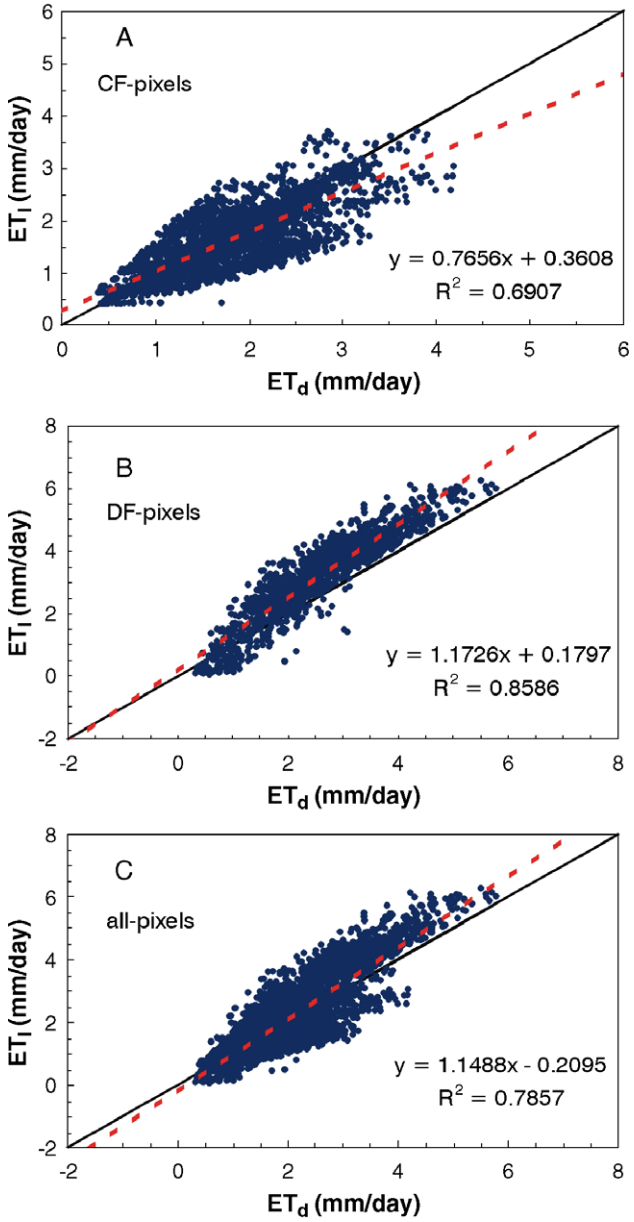

Fig. 3. Lumped (ET_l) versus distributed (ET_d) ET, before correction. Each point represents ET of a single 1-km pixel on a given day (day of year 150 through day of year 250). Are represented: (A) all pixels dominated by the coniferous forest (CF pixels); (B) all pixels dominated by the deciduous forest (DF pixels); (C) all pixels of the watershed.

causing soil moisture and ET to be larger over flat than over bumpy surfaces. Thus, to account for the four effects (land cover, LAI, soil texture, topography), we expressed R as follow:

$$R = R_{lc} \cdot R_{lai} \cdot R_{soil} \cdot R_{top} \tag{2}$$

where R_{lc}, R_{soil}, R_{top}, and R_{lai} are functions that correct ET_l rates as biased following the simplification of land surface complexity within each coarse pixel to a representation of that pixel by the dominant land cover and soil types, and by the average topography and LAI conditions, respectively.

The form of Eq. (2) ensures that each of the four components of R is totally independent from the other three components. It also ensures that we do not need the sub-pixel information of all the four variables (land cover, LAI, soil texture, topography) to be available at the same time to make an ET correction. If for example only land cover sub-pixel information is available to us, R will be reduced to R_{lc}. Similarly, if for example the location for which we want to make an ET correction is completely flat and do not present any topographical variations, R in this case will encompass only three components (R_{lc}, R_{lai}, and R_{soil}) as R_{top} will be equal to 1 and hence eliminated. Another example is that if the location for which we want to make an ET correction is entirely covered by the same vegetation type, R will encompass only three components (R_{lai}, R_{soil}, and R_{top}) as R_{lc} will be equal to 1 and hence eliminated.

The independence of the four components of R in Eq. (2) offers us the possibility to determine each one of them separately by isolating the exclusive effect of the heterogeneity of one of the four variables (e.g., topography) on ET, as we show in the following three sub-sections (Sections 3.3.1, 3.3.2 and 3.3.3).

3.3.1. Land cover correction

If the region or pixel for which we want to correct ET_l is completely flat, having a uniform soil texture and LAI, but an heterogeneous land cover, Eq. (1) will be reduced, as we explained above, to:

$$ET_d = ET_l \cdot R_{lc} \tag{1'}$$

Within each distributed pixel, ET_d may be expressed as:

$$ET_d = ET_1 f_1 + ET_2 f_2 + \ldots + ET_j f_j + \ldots + ET_n f_n = \sum_{i=1}^{n} ET_i f_i \tag{3}$$

where ET_i is the rate of evaporated water by the land cover type i that have a fraction cover f_i.

If each distributed pixel contains a mixture of land cover types, and land cover type j dominates, j will be the land cover of the lumped pixels. Thus, ET_j will represent the evaporation rate of the lumped pixel, and may be replaced by ET_l in Eq. (3). Thereafter, combination of Eqs. (1') and (3) gives:

$$ET_l \cdot R_{lc} = ET_1 f_1 + ET_2 f_2 + \ldots + ET_l f_j + \ldots + ET_n f_n \tag{4}$$

Because $\sum_i f_i = 1$, Eq. (4) may be rewritten as:

$$ET_l \cdot R_{lc} = ET_1 f_1 + ET_2 f_2 + \ldots + ET_l \cdot (1 - f_1 - \ldots - f_{j-1} - f_{j+1} - \ldots - f_n) + \ldots + ET_n f_n \tag{5}$$

Rearranging Eq. (5) yields:

$$R_{lc} = 1 - \left(1 - \frac{ET_1}{ET_l}\right) f_1 - \left(1 - \frac{ET_2}{ET_l}\right) f_2 - \ldots - \left(1 - \frac{ET_n}{ET_l}\right) f_n \tag{6}$$

or:

$$R_{\mathrm{lc}} = 1 - \sum_{i=1}^{n} C_{if}\, f_i \qquad \text{where } C_{ij} = 1 - \frac{\mathrm{ET}_i}{\mathrm{ET}_{\mathrm{l}}};\ i \neq j \tag{7}$$

C_{ij} is a regression coefficient for a non-dominant land cover type i, present in a coarse pixel (1 km in this study) labeled as (or dominated by) land cover type j, and n is the number of non dominant land cover types within that coarse pixel.

The relationships between R_{lc} and land cover type fractions are shown in Fig. 4A–C for the 1-km pixels dominated by CF, and in Fig. 4D–F for the 1-km pixels dominated by DF. It can be seen that for pixels dominated by CF, $\mathrm{ET_d}/\mathrm{ET_l}$ increases with the increase of the DF fraction (Fig. 4A); presumably because ET of DF is higher than ET of CF, so that the elimination of DF fraction in the lumped calculations negatively biases $\mathrm{ET_l}$ of CF pixels. For the same reasons, $\mathrm{ET_d}/\mathrm{ET_l}$ decreases in pixels dominated by DF with the increase of the CF fraction (Fig. 4D). Furthermore, Fig. 4E shows that $\mathrm{ET_d}/\mathrm{ET_l}$ increases with the increase of the MF fraction. This indicates that in this boreal system, the model predicted, in agreement with field observations (Fluxnet-Canada, 2003, p. 39), that a mixed forest may have a higher ET than a deciduous forest as a result of the combined effect of multiple environmental factors (e.g., soil, topography, or other factors).

The coefficients C_{ij} derived from the regressions shown in Fig. 4A–F are given in Table 2, while an example of their derivation is given in Appendix C.1.

3.3.2. LAI correction

R_{lai} was derived based on ET's sensitivity to LAI, as predicted by our model (Fig. 5). Other studies, where other models were used (El Maayar et al., 2002; Pitman, 1994), reported a fairly similar response of ET of coniferous and deciduous forests to LAI variations. We found that the function that best represents the shape of the curves shown in Fig. 5 is:

$$R_{\mathrm{lai}} = \sum_{i=1}^{n} f_i \left[2 - \exp\left(K \frac{\mathrm{LAI}_i - \mathrm{LAI}_{\mathrm{l}}}{\mathrm{LAI}_{\mathrm{l}}} \right) \right] \tag{8}$$

where LAI_l is the leaf area index of the coarse pixel (average leaf area index within the 1-km pixel), LAI_i is the leaf area index of a land cover i within the coarse pixel, f_i is the fraction of the land cover type i within the coarse pixel, and n is the number of existing land cover types within the coarse pixel. K is a parameter that should be adjusted to match the response of ET to LAI variation of a particular land cover type. Our analyses showed that −0.35 represents a reasonable approximation for K, for both coniferous and deciduous forests, although −0.4 and −0.28 would be better approximations for CF and DF, respectively. If only one cover type is present in the coarse

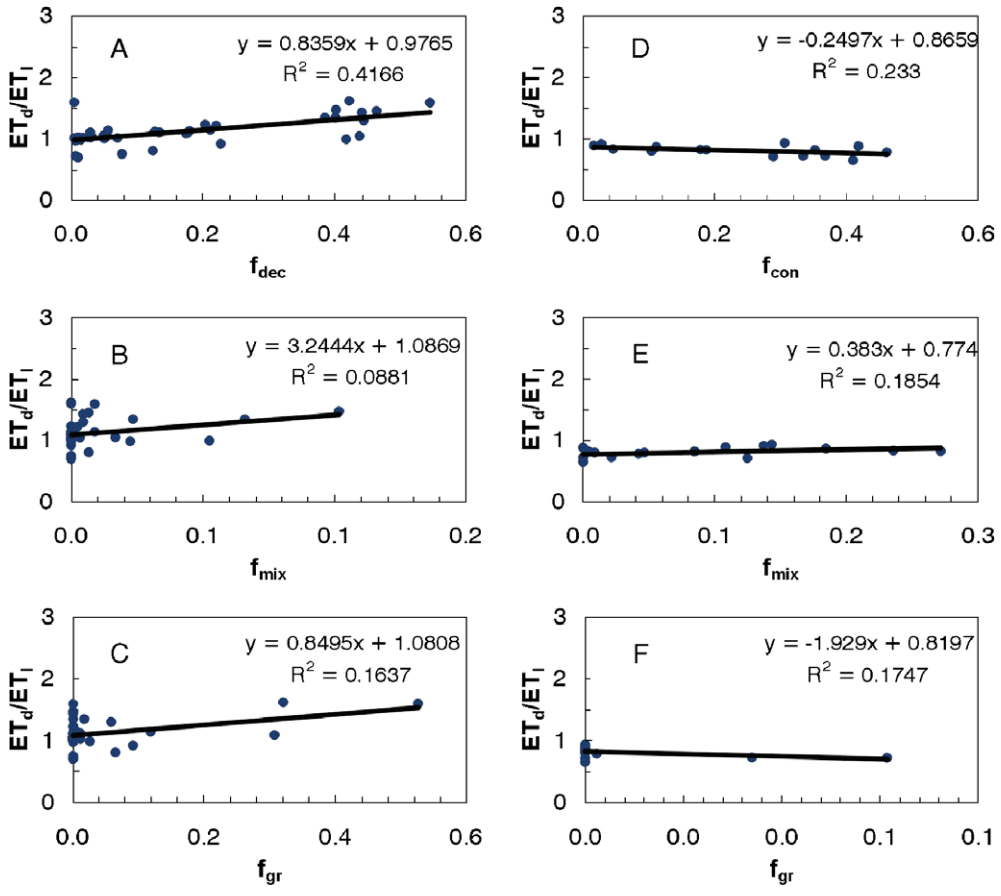

Fig. 4. Variation of average $\mathrm{ET_d}/\mathrm{ET_l}$ as a function of the fraction of non-dominant land cover types in: (A–C) pixels dominated by the coniferous forest (CF pixels); (D–F) pixels dominated by the deciduous forest (DF pixels).

Table 2
C_{ij} coefficients used in the land cover correction component (R_{lc}) of the algorithm

Lumped pixels labeled as coniferous forest			Lumped pixels labeled as deciduous forest		
$C_{dec\text{-}con}$	$C_{mix\text{-}con}$	$C_{gr\text{-}con}$	$C_{con\text{-}dec}$	$C_{mix\text{-}dec}$	$C_{gr\text{-}dec}$
−0.73	−3.64	−1.22	0.56	0.41	3.55

The subscripts con, dec, mix, and gr refer to coniferous forest, deciduous forest, mixed forest, and grasses, respectively.

pixel, f_i will be equal to 1, and the term inside the exponential function becomes null (LAI_i equals LAI_l). Consequently, R_{lai} will be equal to 1.

We opted for the use of Eq. (8) rather than the one proposed in Simic et al. (2004) because it expresses better the non-linearity of the response of ET to LAI variations.

3.3.3. Soil correction

As Earth's distributions of vegetation and climate are strongly correlated, it is well known that a strong correlation between distributions of natural land covers and soil types also exists. In Canada for example, temperate conifer trees most commonly grow further in regions where soil texture contains high proportions of sand materials (Farrar, 1995). Hence, by imposing in lumped calculations a unique (dominant) soil texture for pixels that contain in reality a mixture of land cover types, we inevitably run the risk of associating that dominant soil texture with a land cover type that normally grows further only in locations that are characterized by the presence of another soil texture. For example, if a coarse pixel is dominated by a land cover type A that grows further only in regions of a dominant soil type A, but contains also a non-dominant land cover type B that grows further only in regions of a non-dominant soil type B. Lumped calculation of ET in that pixel will ignore both land cover and soil types B. The use of R_{lc} (Eq. (7)) to correct ET_l will act as an inclusion of the non-dominant land cover type B fraction in ET_l calculation. However, that first ET_l correction (R_{lc}) will need to be further completed by an additional function that links the presence of land cover type B to the presence of soil type B.

In the proposed algorithm, soil correction is driven by the response of ET of each land cover type to different soil textures. In other words, we examined the sensitivity of ET of each land cover type to all the existing soil textural classes within our watershed, to derive a simple methodology that reduces the ET bias due to the use of a unique (dominant) soil type in the lumped calculations. Here, our analyses are limited to the soil texture types present in our studied watershed, but the methodology itself can be applied to any other regions, where sub-pixel soil texture information is available. Thus, we expressed R_{soil} (Eq. (2)) as follows:

$$R_{soil} = \sum_{i=1}^{n} C_{ij}^{soil} \cdot f\,soil_i; \quad \sum_i f\,soil_i = 1 \tag{9}$$

where $fsoil_i$ is the fraction of soil type i (dominant or non-dominant) found within the coarse pixel, and C_{ij}^{soil} is the ratio of ET estimated using a non-dominant soil texture i to the estimated ET using the dominant soil texture j. n is the number of soil types present within the coarse pixel. For our watershed (Fig. 6A–D), our analyses yielded the average values of C_{ij}^{soil} given in Table 3. A discussion on C_{ij}^{soil} coefficients is given in the last section of this paper.

An Example of calculation of C_{ij}^{soil} coefficients is given in Appendix C.2.

3.3.4. Topography correction

Topography has a major influence on surface water budget components, such as precipitation (Daly et al., 1994), snow cover distribution (Essery, 2003; Walland & Simmonds, 1996), available soil water capacity and soil moisture (Grant, 2004; Zeng et al., 1996), runoff generation (Haddeland et al., 2002), and evapotranspiration (Kang et al., 2004). TerrainLab simulates the transfer of water between adjacent pixels that have different elevations. The amount of water and the required time for its transfer from one pixel to the other are non-linear functions of the difference between their elevations and aspects (Chen et al., 2005). Consequently, the use of average topography in lumped calculations is similar to imposing a linear relationship between ET and surface topography, which is incorrect (an example is given in the 2nd paragraph of Section 3.3). Therefore, our objective is the derivation of a simple function that reduces the bias that results from the use of average topography in lumped calculations of ET. We also seek that the proposed function will be simple and flexible enough to be easily applicable under contrasting environmental conditions.

To isolate the effect of topography on ET, we firstly made three runs at a 1-km resolution for the pixels dominated either by CF or DF. In each of the three runs, the latter vegetation types were assumed to grow on one of the three soil textural types found within the watershed area (loamy sand, silty clay or peat). Secondly, we performed three other runs at a 30-m resolution for the same corresponding distributed pixels (1 km), assuming again an unique soil texture in each run. In the 30-m resolution runs furthermore, a unique vegetation cover was prescribed for each distributed pixel. CF and DF were prescribed for the distributed pixels where CF and DF dominate, respectively. As

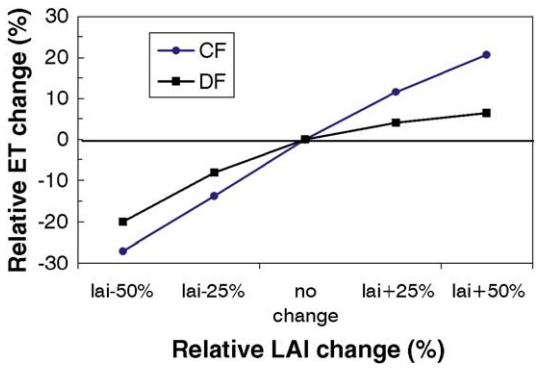

Fig. 5. Sensitivity of ET to changes in leaf area index (LAI) of coniferous (CF) and deciduous (DF) forests.

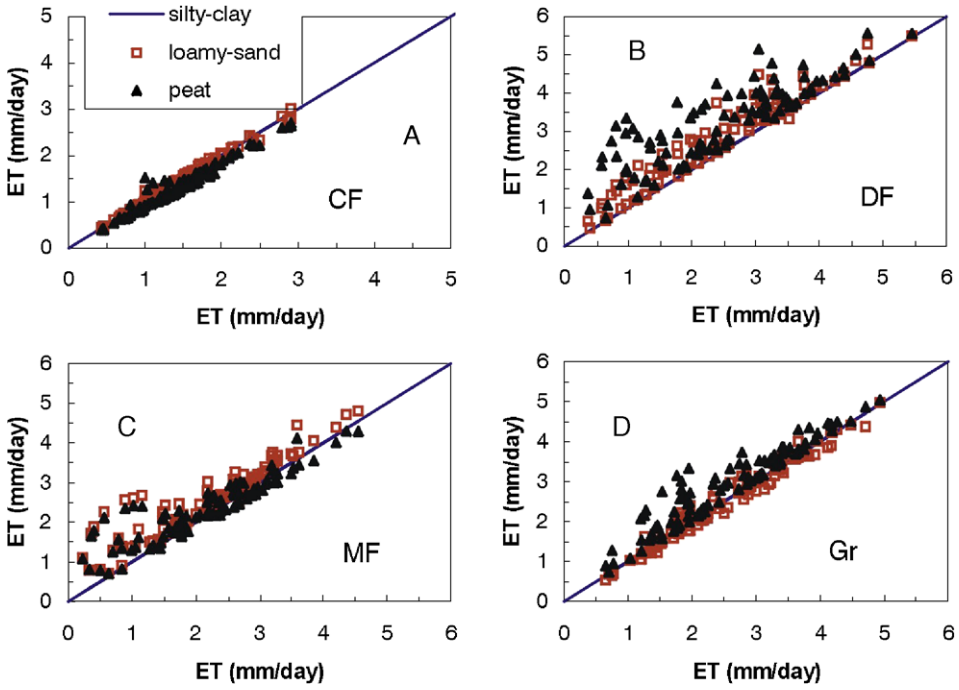

Fig. 6. Sensitivity of ET to soil texture as predicted by TerrainLab, for: (A) coniferous forest (CF); (B) deciduous forest (DF); (C) mixed forest (MF); (D) grasses (Gr).

land cover and soil texture were similar in both lumped (1 km) and distributed (30 m) runs, their effects were thus eliminated. Our choice of making three separate runs where each run corresponds to a soil type was dictated by the fact that CF and DF grow up over all the three soil types found in our watershed (silty-clay, loamy-sand, and peat) (Plate 1), although the two vegetation types are mainly found in areas where loamy-sand (for CF) and silty-clay (for DF) soils dominate.

Our results illustrate that the response of ET_d/ET_l to topographical variations depends on the soil texture (Fig. 7A–F), which is not surprising. While ET_d/ET_l decreases as the elevation range within the coarse pixels increases when CF and DF grow further on silty-clay soils (Fig. 7C,D) and peat soils (Fig. 7E,F), its variation remains very low when the two vegetation types grow on the loamy-sand soil (Fig. 7A,B). Elevation range refers to the difference between the highest and the lowest elevations of the 30-m pixels found within each coarse pixel (1 km). The decrease of ET_d/ET_l as a function of the elevation range in silty-clay and peat soil cases was more or less expected because lumping results in soil moisture to be more uniform than reality, which reduces moisture stress and causes ET_l to be positively biased. Furthermore, the rank coefficient correlation test of Spearman at the 95% level (Keller & Warrack, 1997) applied to the results shown in Fig. 7C–F confirmed the existence of a statistically significant relationship between ET_d/ET_l and elevation range. $r(\sqrt{R^2})$ values for CF (Fig. 7C,E) and DF (Fig. 7D,F) were found to be larger than the critical values. In the loamy-sand soil case (Fig. 7A,B), ET_d/ET_l was almost insensitive to the elevation range changes as it was also confirmed by the rank coefficient correlation test of Spearman at the 95% level, although the lumping caused a small negative bias ($ET_d < ET_l$). The latter response resulted from the combination of two effects: (i) Firstly, the high hydraulic conductivity of loamy-sand soils causes water to infiltrate during rainy events very quickly, which dramatically decreased the effect of topographical variations on ET_d/ET_l; (ii) Secondly, soil moisture was generally lower in lumped runs than in distributed runs because the infiltrated water was more efficiently distributed throughout the soil profile in the distributed case. This difference in soil water distribution resulted from a longer period of water transfer from the surface to the deep soil in the distributed case than in the lumped case, as soil in some areas with high elevations within the distributed coarse pixels could be significantly deeper than average. In the distributed case, soil in depressed areas also tends to accumulate water, giving rise to higher ET at these locations, and this spatial process is missed in the lumped calculation. Interestingly, using another hydrological model (RHESSys) that accounts for topographical effects on surface hydrology, Mitchell et al. (2005) have also reported that distributed calculations yielded larger ET rates than those obtained from lumped calculations in a grassland ecosystem

Table 3
C_{ij}^{soil} coefficients used in the soil correction component (R_{soil}) of the algorithm

	$C_{sc\text{-}ls}^{soil}$	$C_{p\text{-}ls}^{soil}$	$C_{lc\text{-}sc}^{soil}$	$C_{p\text{-}sc}^{soil}$	$C_{ls\text{-}p}^{soil}$	$C_{sc\text{-}p}^{soil}$
Lumped pixels labeled as coniferous forest	1.02	0.92	0.98	0.91	1.09	0.98
Lumped pixels labeled as deciduous forest	1.14	1.30	0.88	1.14	0.77	0.88

i and *j* represent the non-dominant and the dominant soil types, respectively. The subscripts sc, ls, and p denote silty-clay, loamy-sand and peat soils, respectively. $C_{sc\text{-}ls}^{soil}$ represents the ratio of obtained ET when the soil is silty-clay to the obtained ET when the soil is loamy-sand; and so on (see text for explanation). $C_{sc\text{-}sc}^{soil}$, $C_{ls\text{-}ls}^{soil}$, and $C_{p\text{-}p}^{soil}$ are all equal to 1.

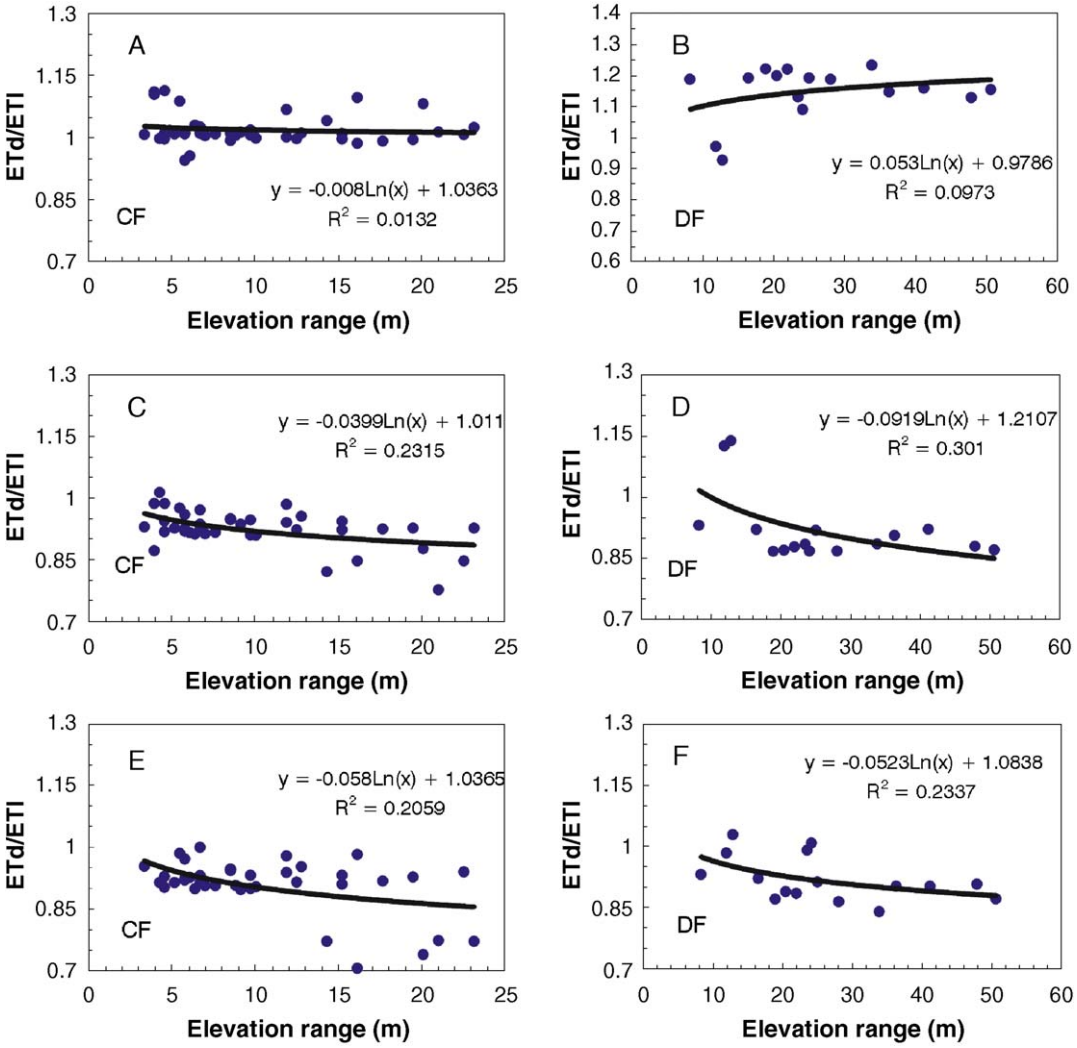

Fig. 7. Variation of ET_d/ET_l as a function of elevation range within the 1-km pixels, when both conifer and deciduous forests grow further on: (A,B) loamy-sand soil; (C,D) silty-clay soil; (E,F) peat soil.

located in the Prairies Grasslands Natural Region of Canada, where soil contains a high proportion of sand.

Based on these results (Fig. 7A–F), we used the following simple equation to express R_{top} to correct for the effects of topographical variations within the coarse pixels on ET calculations:

$$R_{top} = a\ln[\text{elevrange}] + b \quad (10)$$

where elevrange is the elevation range within the coarse pixel which can be obtained from high resolution DEMs, ln is the natural logarithm, and a and b are coefficients to be adjusted for each land cover and soil type, as illustrated in Fig. 7A–F. Approximate values of a and b are those shown in Fig. 7A–F. Note that for small values of elevrange, R_{top} converges toward 1. Eq. (10) is therefore considered to be equal to 1 for values of elevrange that are equal or smaller than e (~2.71). A discussion on a and b coefficients can be found in the Section 4 of this paper.

We choose the elevation range rather than other variables for the topographical correction for the following reason: (i) Our objective is to provide the simplest and the most practical possible algorithm to the user. If, for instance, we consider the slope variable in the topographical correction, we necessarily need to add another additional component of this topographical correction that includes effect of the aspect on ET. This is because water flows between two points with different elevations could depend as much on slope as on aspect. After several analyses, we found that the use of a single simple component in the topographical correction that takes into account the elevation difference (or range when we talk about a watershed) is straightforward because it implicitly includes all the combined effects of slope and aspect; and (ii) In practice, it is very often much easier to find elevation data than aspect and slope data, especially if we are interested in correcting ET estimates made at regional or larger scales.

3.3.5. Corrected versus uncorrected ET

Regressions between daily values of watershed-average ET_d, ET_l, and corrected ET_l are shown in Figs. 2A–C and 8A–C. While before correction, ET_l of CF pixels differs only slightly from ET_l after correction (Figs. 2A and 8A), a noticeable

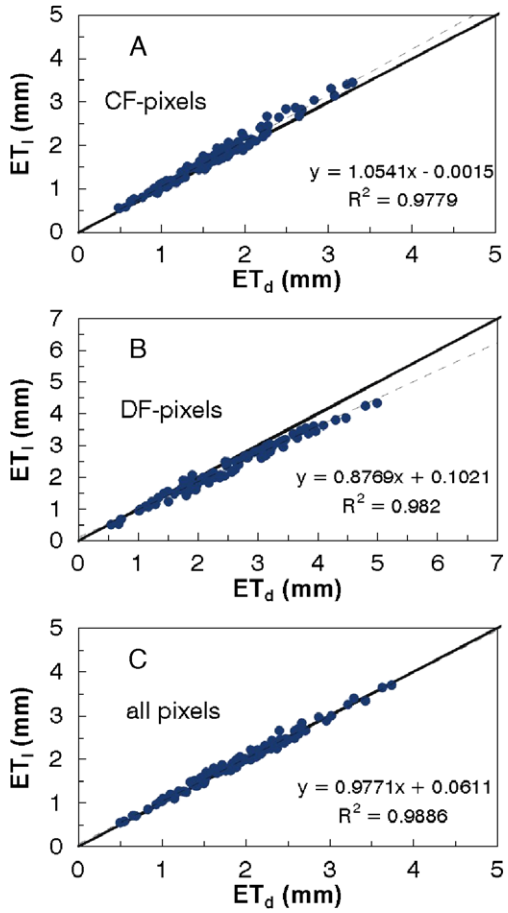

Fig. 8. Regression between lumped (ET_l) and distributed (ET_d) daily values of ET (day of year 150 through day of year 250), after correction. Each point represents obtained average ET in a given day, over: (A) all pixels dominated by the coniferous forest (CF pixels); (B) all pixels dominated by the deciduous forest (DF pixels); (C) all pixels of the watershed.

improvement was obtained for DF pixels (Figs. 2B and 8B). In terms of percentage, the application of algorithm yielded a reduction in the mean bias error (MBE) of average ET_l from 8% to 5% for the coniferous forest, from 24% to 8% for the deciduous forest, and from 4% to less than 1% for the entire watershed (Table 1).

Regression analyses made using daily values of ET_l and ET_d as obtained for every 1-km pixel of the watershed (58 pixels) through the entire period of the study (101 days) show that the algorithm considerably reduced the ET_l bias of both coniferous and deciduous forests (Fig. 3A–C vs. Fig. 9A–C), which indicates a significant improvement of the spatial variability of ET_l within the watershed. For illustration, the spatial variability of time-average (days of year 150–250) values of ET_d, and the corresponding uncorrected and corrected ET_l along all the watershed coarse pixels (58 at 1-km resolution) are shown in Fig. 10A–C. These figures (Fig. 10A–C) indicate an important improvement of the spatial variability of ET_l as the coefficients of variation established for ET_d, uncorrected ET_l and corrected ET_l to 0.25, 0.40 and 0.22, respectively.

Our analyses indicate that lumping causes a larger bias during the dry period than during the wet period (Fig. 11A–C). Early in the growing season (around day number 50 in Fig. 11A–C), the ET bias is low even though the weather is dry, because the soil moisture is still high due the important soil water recharge by snow melt that occurs during that period. Furthermore, Fig. 11A–C shows that the algorithm operates better during the dry period.

Fig. 12A illustrates the contribution of each algorithm component to R (Eq. (2)). In our watershed case study, the soil texture and LAI corrections were minimal, and land cover and topography corrections were almost of equal importance. In average, R_{soil} and R_{lai} had only a minor effect on ET_l (less than 1% correction) on both coniferous and deciduous forests. On

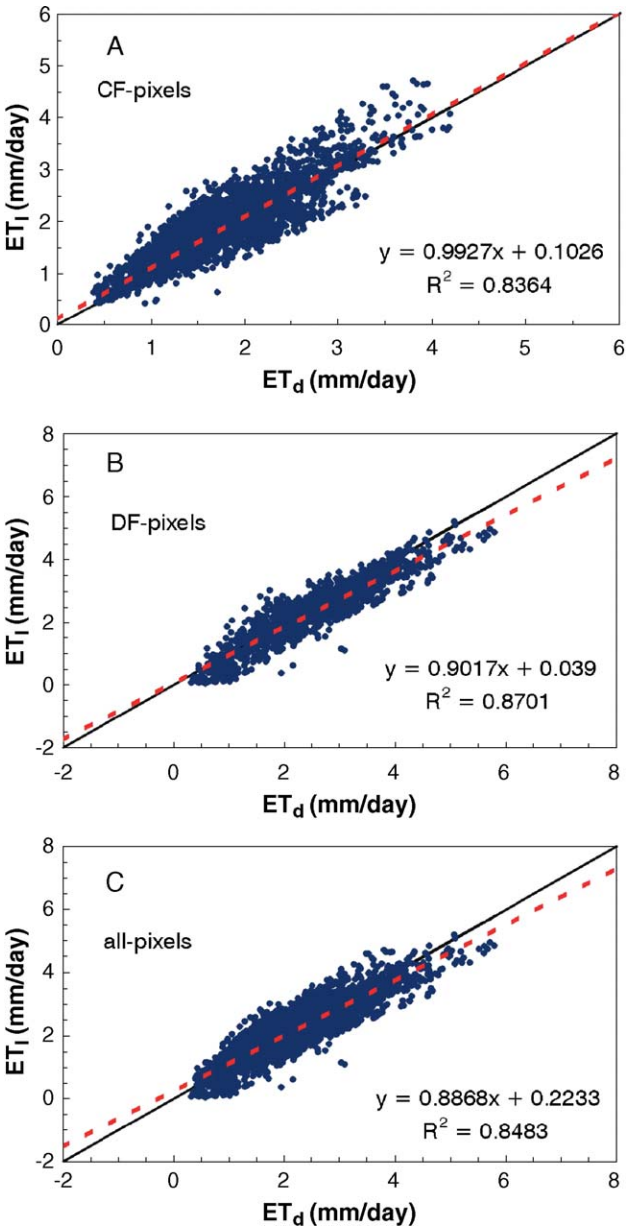

Fig. 9. Lumped (ET_l) versus distributed (ET_d) ET, after correction. Each point represents ET of a single 1-km pixel in a given day (day of year 150 through day of year 250). Are represented: (A) all pixels dominated by the coniferous forest (CF pixels); (B) all pixels dominated by the deciduous forest (DF pixels); (C) all pixels of the watershed.

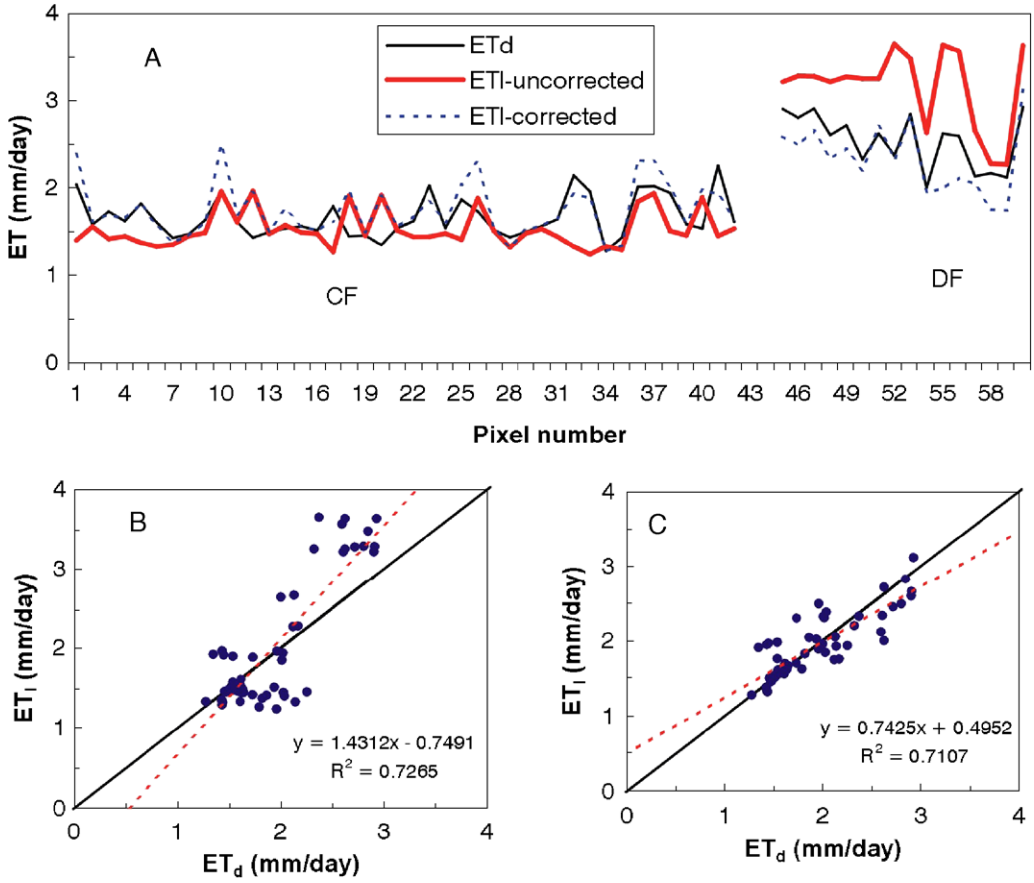

Fig. 10. (A) Comparison of the spatial variability of ET_d and ET_l before and after correction, for coniferous (CF pixels) and deciduous (DF pixels) forests. (B) and (C) show the regressions between lumped (ET_l) and distributed (ET_d) values of ET obtained at each of the 1-km pixels of the watershed before and after correction, respectively.

average, R_{lc} increased ET_l of coniferous forest by 16% and decreased ET_l of deciduous forest by 19%, while R_{topo} decreased ET_l of coniferous and deciduous forests by 1% and 7%, respectively.

4. Discussion and conclusion

Remote sensing-based ecosystem models are emerging as powerful tools capable of estimating ET over large regions, at relatively high resolutions. These models that are able to assimilate a mixture of information on surface boundary conditions, can now provide us with regional, continental or even global ET maps at spatial resolutions as high as 1 km (Liu et al., 2003; Running et al., 2000). However, because landscape heterogeneity could still be considerable even at that resolution, a simple algorithm that correct estimated ET at coarse spatial resolutions by using sub-pixel information on land surface heterogeneity was proposed in this study. In our case study, a watershed located in the Canadian boreal forest, the algorithm demonstrated its ability to improve significantly temporal and spatial averages of estimated ET, and most importantly, ET's spatial distribution. One may ask, however, whether our approach that was derived based on two fixed resolutions, is applicable to images with varying resolutions. The proposed algorithm is, in fact, scale-independent, and is intended to be exclusively sensitive to the distribution of surface characteristics within coarse pixels. Furthermore, although the performance of our algorithm depends closely on the judicious choice of some coefficients derived using a single model results such as C_{ij} (Eq. (7)), C_{ij}^{soil} (Eq. (9)), and a and b (Eq. (10)), values of these coefficients may be easily adjusted for any other model by following the simple procedure we adopted for their derivation (i.e., sensitivity analyses). Adjustment of C_{ij}, C_{ij}^{soil}, and a and b coefficients to correct coarse resolution ET estimations made by other models is even mandatory and could be referred to as a calibration of the algorithm. For example, to correct coarse resolution ET calculations made by any ecosystem model over a region as large as Canada, C_{ij}^{soil} coefficients could be inferred by looking at ET's sensitivity of a particular land cover type to different soil textures within that model (see Fig. 6), in few specific points distributed within that region. It is worth noting, however, that most process-based models use very similar set of relationships to describe ecosystem physical and physiological processes. We, therefore, anticipate that C_{ij}, C_{ij}^{soil}, and a and b should not vary substantially between that class of models. Furthermore, with the proliferation of tower flux measurements over the major world's biomes, some of these measurements could be used in the near future to derive accurate values of C_{ij}^{soil} coefficients. Potentially, a and b coefficients (Eq. (10)) might be also much more refined by testing the proposed algorithm over

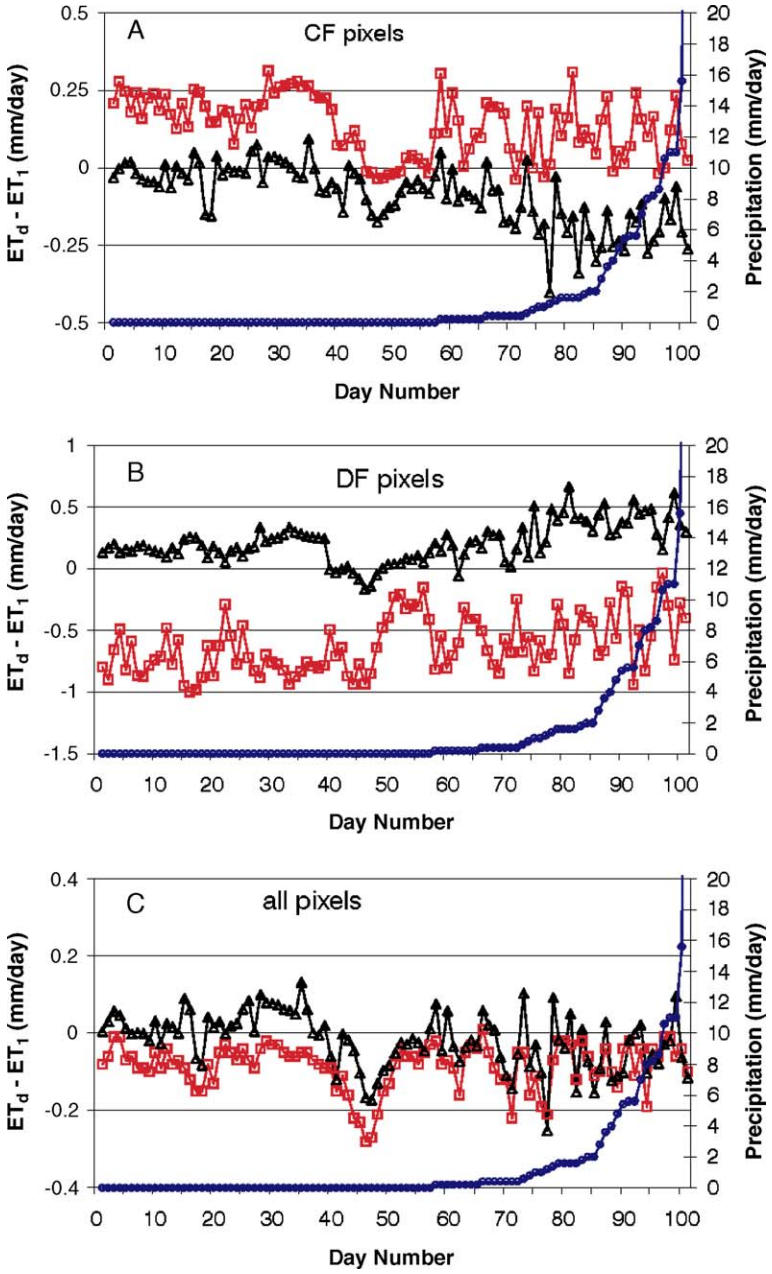

Fig. 11. Effect of wetness/drought conditions on lumped ET, for conifer forest pixels (A), deciduous forest pixels (B), and the entire watershed (C). Square and triangle symbols refer to the difference between ET_d, and uncorrected and corrected ET_l, respectively. Circle symbols are for precipitation. The day number in the *x*-axis refers to days of years 150–250 sorted out by ascending precipitation rates.

regions with more complex topography (e.g., mountains) than the watershed studied here. It may be effective to refine two sets of *a* and *b* coefficients that could be applied separately to relatively flat and mountainous regions. More generally, consistently with results of other studies (e.g., Wood, 1997), this study showed that lumping may yield more or less important ET bias depending on the wetness/drought conditions. That is, in regions with pronounced precipitation cycle, it might be more appropriate to use two sets of parameters relatively to the wet and dry periods. Moreover, because the four components of the algorithm are completely independent, its application does not require that sub-pixel information on the four surface characteristics investigated in this study should be available at the same time. For instance, if only sub-pixel information on soil cover is available, only R_{soil} would be used to correct lumped ET estimates, as R in Eq. (2) will be reduced to R_{soil}. Similarly, if only sub-pixel information on land cover is available, only R_{lc} would be used to correct lumped ET. This term independency contributes to the practical aspect of the proposed algorithm.

For our analyses, two separate simulations (distributed [30-m resolution] and lumped [1-km resolution]) were made to examine the effects of the simplification of land surface to a juxtaposition of uniform coarse pixels on ET calculations over large areas. The ratio ET_d/ET_l derived from results of the two simulations gave us an idea on the relative ET_l bias. Most of

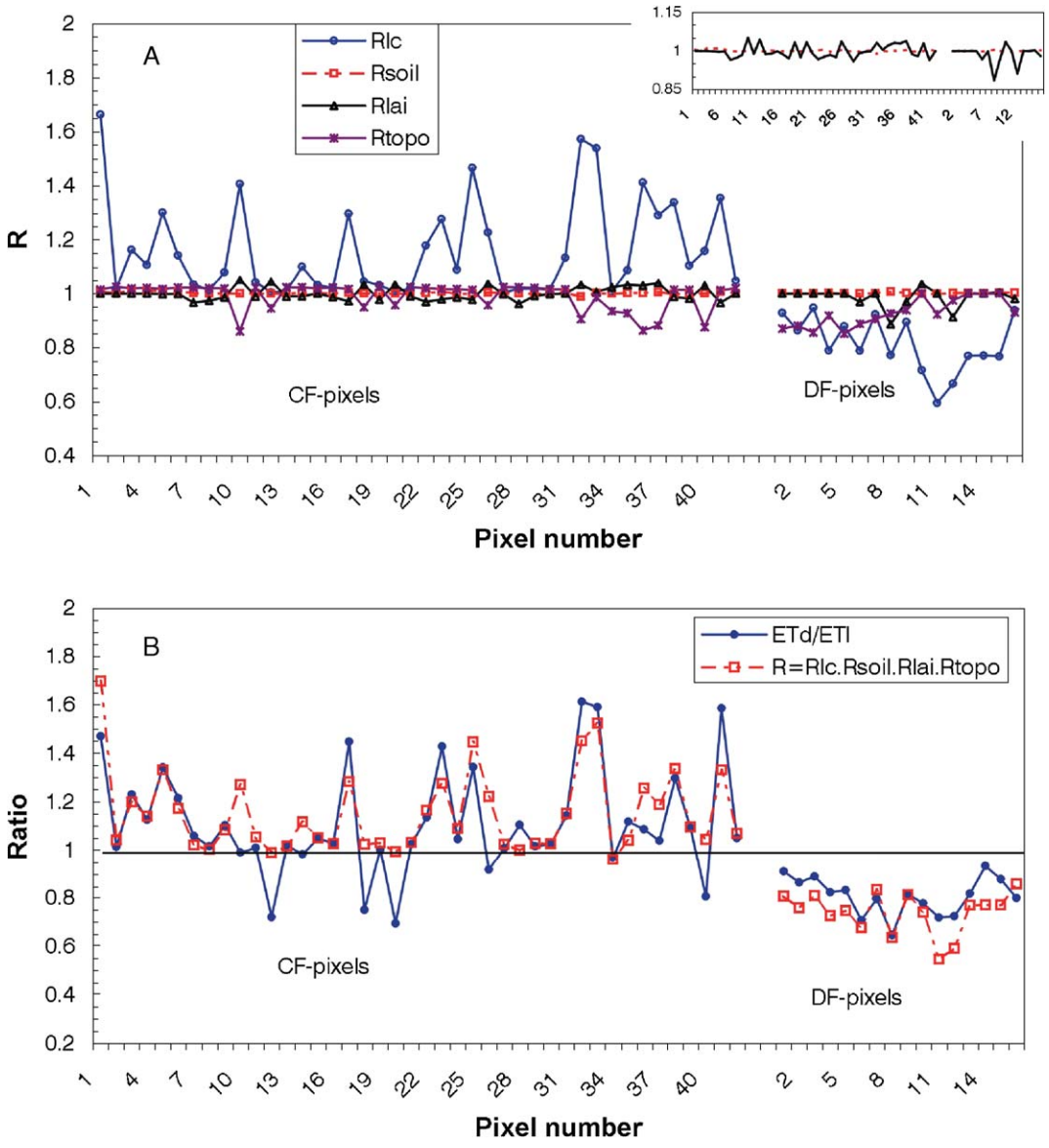

Fig. 12. Illustration of (A) the contribution of each algorithm component (Eq. (2)) to the total correction (R) at each 1-km pixel. A zoom of the [0.85, 1.15] portion of the y-axis is also shown (inset figure) to better illustrate R_{soil} and R_{lai} contributions; (B) the comparison of calculated ET_d/ET_l using available data at 30-m and 1-km resolutions, and estimated ET_d/ET_l (R) by the algorithm.

time in practice, however, only ET_l calculations are possible. Thereby, the objective of our algorithm could be referred to as "*the modelling*" of ET_d/ET_l ratio, using subpixel information. In Fig. 12B, we compared the average "*real*" (ET_d/ET_l) and the average "modelled (R; Eq. (2))" ratios along all the watershed pixels. It is shown that our algorithm (R) reproduced reasonably well the expected ET_d/ET_l ratio, although differences between these two ratios still exist for several potential reasons. Additionally, we should note that our modeled results and the subsequent derived coefficient (e.g., C_{ij}) are not affected by the fact that the measured meteorological data in our study were provided from one station only, for the following reasons: (a) the watershed is small (10.8 km × 10.8 km). Thus, only marginal meteorological changes might be expected 5.4 km away in each direction from the meteorological station that is located in the center of the watershed; (b) the topography of the watershed (as we mentioned in Section 2.2) has low relief (Nakane et al., 1997), which ensures homogeneous meteorological conditions within the watershed area.

One may also ask about the applicability of the proposed approach in different Earth's locations in conjunction with the ability of current remote sensing techniques to provide us with land cover maps at very high spatial resolutions (e.g. 30 m). Currently, in fact, this remains an important challenge, though the work of DeFries et al. (1997) brought up the possibility for a better land cover characterization at very high spatial resolutions, using what they had named the soft-labeling (also known as fuzzy-labeling) approach. The latter approach that allows for the derivation of the fractions of major land cover types within a given pixel, contrasts with the hard-labeling (or discrete-labeling) procedure that forces a pixel to a unique land cover type. Recently, Canters et al. (2002) demonstrated the

applicability of the soft classification through the derivation of a 1-km resolution land cover map of Europe, where the fraction cover of each land cover type within each pixel is given. Nevertheless, the soft classification approach still suffers an important limitation inherent to the difficulty to achieve spectral unmixing as the unique dimensions of optical remote sensing are generally smaller than the dimension of surface variability (Verstrate et al., 1996). Therefore, as pointed-out by Chen (1999), a greater effort in remote sensing science should address the question of mapping land surface characteristics at spatial resolutions comparable to surface variability, if we take the spatial scaling as a serious issue in quantitative remote sensing applications. An additional effort should focus on the development of high resolution maps of soil texture and surface topography.

Finally, we anticipate that the use of our approach would allow for improving estimates of regional carbon fluxes as several studies illustrated that the use of coarse spatial resolutions in ecosystem models introduce much larger biases on carbon fluxes calculations (e.g., NPP and respiration) than on ET calculations (Kang et al., 2003; Kimball et al., 1999; Turner et al., 1996). Moreover, while our study explicitly accounted for important factors that affect scaling behaviour such as land cover and surface topography, other potentially important factors such as spatial distributions of stand age, disease and soil nutrients were ignored, but these factors could be addressed in similar manners in future investigations.

Acknowledgement

This study is part of the Fluxnet Canada Research Network modeling activities supported by the Natural Science and Engineering Council of Canada and the Canadian Foundation of Climate and Atmospheric Sciences. The interface of TerrainLab was built by Mr. Andriy Budyko. Technical assistance of Weimin Ju and Mingzhen Chen is appreciated. We thank Oliver Sonnentag for useful comments on a previous version of the manuscript, and Abdelwahed Boutahor for his careful English editing. We thank three anonymous reviewers for helpful and fruitful comments and suggestions.

Appendix A. Performance of TerrainLab

The ability of the model to reproduce key hydrological processes, such as ET, soil moisture and water table fluctuations at our watershed is discussed in details in Chen et al. (2005), where the importance of modeling hydrological processes as influenced by topography is shown. Over the 1994 growing season, Chen et al. (2005) found that the model predicted an ET (2.1 mm/day) that is in good agreement with the measured ET (2.07 mm/day) as reported by Jarvis et al. (1997). Predicted ET rates are also in good agreement with the measured rates during three intensive field campaigns of the 1994's growing season period (Patty et al., 1997). Predicted values are 2.31, 2.71, and 1.5 mm/day while measured values were 2.26, 3.32, and 1.44 mm/day during the May 24–June 4, July 19–July 29, and September 8–17 periods, respectively. Furthermore, Chen et al.'s analyses showed that there was no statistically significant difference between the temporal patterns of measured and predicted data. Comparison of predicted and measured soil moisture near the flux tower (Peck et al., 1997) yielded also good agreement as the predicted values were within 10% range of the measured values. Interestingly, moreover, water loss through saturated subsurface flow during the period of our study accounted for about 6% of total precipitation near the flux tower with a very moderate topographical variation within 150 m of the tower. Further analyses also showed that the model predicts adequately water table fluctuations, and spatial and temporal variations of soil water regimes at both lowland and upland locations (Chen et al., 2005).

During the last decade, several studies have focused on the test and the application of the different components of the model, under different environmental conditions. For instance, Storck et al. (1998, 1999) and Whitaker et al. (2003) showed that the Distributed Hydrology Soil Vegetation (DHSV) component (Wigmosta's component) that forms the central structure of TerrainLab predicts successfully streamflow in temperate forests and mountainous regions of the South-Western Canada (British Columbia) and North-Western United States (Washington). Nijssen, Haddeland et al. (1997) demonstrated the ability of that same component (DHSV) to predict accurately the surface hydrology of a boreal forest. Alila and Beckers (2001) went further by using that sub-component of TerrainLab for hydrologic forest management issues in Western Canada (British Columbia), while VanShaar et al. (2002) used that component to examine the effects of land use changes on the hydrology of the Columbia river basin. There exist nearly thirty studies that have devoted to the validation and the application of the different components of the model. Therefore, we are using a model that has been very carefully and intensively tested and validated by different research groups over contrasting environmental conditions, including our watershed conditions.

Appendix B. Data preprocessing

Various spatial datasets are preprocessed as inputs to the model. They include: (i) slope and aspect derived from a digital elevation model (DEM) dataset (16-bit unsigned integer raster file) for each pixel of the watershed with a spatial resolution of 30 m × 30 m using ARCGIS; (ii) meteorological data including precipitation, maximum, minimum and mean air temperature, humidity, and radiation. These variables were measured at the OBS flux-tower site (Jarvis et al., 1997) and treated the same for all pixels within this small watershed; (iii) land cover and LAI maps derived from a Landsat imagery which was geometrically and radiometrically corrected. As part of the image processing, the digital numbers (DN) of the visible and infrared bands are converted into radiance and reflectance after an atmospheric correction procedure. Cihlar et al.'s (1999) land cover classification was used, and LAI was calculated using the algorithms of Chen and Cihlar (1996); and (iv) soil attributes, including texture and water holding capacity, obtained from a soil map at a scale of 1:1,000,000 (Acton et al., 1991; De Jong et al., 1984).

The water table and soil moisture fields before the growing season were initialized using the TOPMODEL principle (Beven & Kirkby, 1979; Kirkby, 1975). The wetness index ($W_{i,j}$) for a pixel (i,j) (Beven & Kirkby, 1979) was first calculated as:

$$W_{ij} = \ln\left(\frac{A_{ij}}{\tan\beta_{ij} + 0.05}\right) \quad \text{(A1)}$$

where $A_{i,j}$ is the contributing area calculated from the DEM using the ARCGIS FLOWACCUMULATION command, and $\beta_{i,j}$ is the slope. ln is the natural logarithm.

The initial water table ($W_{t,i,j}$) was then linearly related to the wetness index:

$$W_{t_{i,j}} = \bar{W}_t + m(W_{i,j} - \bar{W}) \quad \text{(A2)}$$

where $\bar{W}_t$ is the mean water table taken as 0.35 m determined through a spin-up calculation for one year; and $\bar{W}$ is the mean wetness index determined to be 4 from the W image, and m was set at 0.7 m (Beaujouan et al., 2002). The soil moisture content in the unsaturated zone is set to 70% of the field capacity at the beginning of the growing season for all pixels.

In this study, all input data were spatially re-sampled to a common 30 m × 30 m spatial resolution, to be compatible with Landsat TM images.

Appendix C

C.1. Example of calculation of land cover coefficients, C_{ij} (Eq. (7))

In Fig. 4A (CF is the dominant land cover type), $R_{lc} = 0.84 f_{dec} + 0.98$. Eq. (7) indicates, moreover, that R_{lc} is expressed as: $R_{lc} = 1 - C_{dec\text{-}con} \cdot f_{dec}$. Combination of the two above equations yields: $C_{dec\text{-}con} = (1/f_{dec}) \cdot [1 - (0.84 \cdot f_{dec} + 0.98)]$. $C_{dec\text{-}con}$ (−0.73; Table 2) is the average $C_{dec\text{-}con}$ calculated for f_{dec} that varies between 0 and 0.49; i.e., all values that f_{dec} may have within a coarse pixel where CF dominates. All other C_{ij} values were derived in a similar manner.

C.2. Example of calculation of soil coefficients, C_{ij}^{soil} (Eq. (9))

Assuming: (i) within a 1-km pixel, CF and loamy-sand texture are the dominant land cover and soil types, respectively; and (ii) within that coarse pixel, the fraction of loamy-sand, silty-clay and peat soils are 0.7, 0.2 and 0.1, respectively.

In lumped calculations, the non-dominant soil types (silty-clay and peat) will be ignored, which would bias the calculation of ET. To apply the soil correction, by taking into account the real fraction of each soil type that is present within the coarse pixel (1 km), R_{soil} will be calculated using Eq. (9) as:

$$R_{soil} = C_{ls-ls}^{soil} \cdot f\,soil_{ls} + C_{sc-ls}^{soil} \cdot f\,soil_{sc} + C_{p-ls}^{soil} \cdot f\,soil_{p}$$

which yield using Table 3:

$$R_{soil} = 1 \times 0.7 + 1.02 \times 0.2 + 0.92 \times 0.1$$

1, 1.02 and 0.92 represent the $C_{ls\text{-}ls}^{soil}$, $C_{sc\text{-}ls}^{soil}$ and $C_{p\text{-}ls}^{soil}$ values, respectively.

References

Alila, Y., & Beckers, J. (2001). Using numerical modelling to address hydrologic forest management issues in British Columbia. *Hydrological Processes*, *15*, 3371–3387.

Acton, D. F., Padbury, G. A., & Shields, J. A. (1991). *Soil Landscapes of Canada-Saskatchewan Digital Map Data; Scale 1 : 1000000*; CanSIS No. SK018200, version 90.11.30; CLBRR Archive, Agriculture Canada, Research Branch, Ottawa, Canada. (CLBRR Contribution No. 91-107D).

Arora, V. K., Chiew, F. H. S., & Grayson, R. B. (2001). Effect of sub-grid scale variability of soil moisture and precipitation intensity on surface runoff and streamflow. *Journal of Geophysical Research*, *106*(D15), 17073–17091.

Avissar, R., & Pielke, R. A. (1989). A parameterization of heteregenous land surfaces for atmospheric numerical models and its impact on regional meteorology. *Monthly Weather Review*, *117*, 2113–2136.

Band, L. E., Patterson, P., Nemani, R. R., & Running, S. W. (1993). Forest ecosystem processes at the watershed scale: 2. Adding hillslope hydrology. *Agricultural and Forest Meteorology*, *63*, 93–126.

Band, L. E., Peterson, D. L., Running, S. W., Coughlan, J. C., Lammers, R., Dungan, J., et al. (1991). Ecosystem processes at the watershed level: Basis for distributed simulation. *Ecological Modeling*, *56*, 171–196.

Beaujouan, V., Durand, P., Ruiz, L., Aurousseau, P., & Cotteret, G. (2002). A hydrological model decicated to topography-based simulation of nitrogen transfer and transformation: Rationale and application to the geomorphology-denitrification relationship. *Hydrological Processes*, *16*, 493–507.

Beven, K. J., & Kirkby, M. J. (1979). A physically-based variable contributing area model of basin hydrology. *Hydrological Sciences Bulletin*, *24*, 43–69.

Bonan, G. B, Levis, S., Kergoat, L., & Oleson, K. W. (2002). Landscapes as patches of plant functional types: An integrating concept for climate and ecosystem models. *Global Biogeochemical Cycles*, *16*, 2, doi:10.1029/2000GB001360.

Bonan, G. B., Pollard, D., & Thompson, S. L. (1993). Influence of subgrid-scale heterogeneity in leaf area index, stomatal resistance, and soil moisture on grid-scale land-atmosphere interactions. *Journal of Climate*, *6*, 1882–1897.

Bonan, G. B., & Shugart, H. H. (1989). Environmental factors and ecological processes in boreal forests. *Annual Review of Ecology and Systematics*, *20*, 1–28.

Boone, A., & Wetzel, P. J. (1998). A simple scheme for modeling sub-grid soil texture variability for use in an atmospheric climate model. *Journal of the Meteorological Society of Japan*, *77*(1), 317–333.

Branfireun, B. A., & Roulet, N. T. (1998). The baseflow and stormflow hydrology of a Precambrian shield headwater peatland. *Hydrological Processes*, *12*, 57–72.

Campbell, G. S., & Norman, J. M. (1998). *An introduction to environmental biophysics*, 2nd edition : Springer-Verlag. 286 pp.

Canters, F., Swinnen, E., Eerens, H., & Van de Voorde, T. (2002). Estimation of land-cover proportions at the subpixel level from 1-km SPOT-VGT data. *Proceedings of the fifth international symposium on spatial accuracy assessment in natural resources and environmental sciences, July 10-12, Melbourne* (pp. 66–74).

Chen, J. M. (1999). Spatial scaling of a remotely sensed surface parameter by contexture. *Remote Sensing of Environment*, *69*, 30–42.

Chen, J. M., Chen, X., Ju, W., & Geng, X. (2005). A remote sensing-driven distributed hydrological model: Mapping evapotranspiration in a forested watershed. *Journal of Hydrology*, *305*, 15–39.

Chen, J. M., & Cihlar, J. (1996). Retrieving leaf area index of boreal conifer forests using Landsat TM images. *Remote Sensing of Environment*, *55*, 153–162.

Chen, J. M., Rich, P. M., Gower, S. T., Norman, J. M., & Plummer, S. (1997). Leaf area index of boreal forests: Theory, techniques, and measurements. *Journal of Geophysical Research*, *102*(D24), 29429–29443.

Cihlar, J., Beaubien, J., Latifovic, R., & Simard, G. (1999). *Land cover of Canada 1995 Version 1.1*. Digital Data Set Documentation. Natural Resource Canada, Ottawa, Ontario.

Daly, C., Neilson, R. P., & Phillips, D. L. (1994). A statistical-topographic model for mapping climatological precipitation over mountainous terrain. *Journal of Applied Meteorology*, *33*, 140−158.

De Jong, R., Shields, J. A., & Sly, W. K. (1984). Estimated soil water reserves applicable to a wheat-fallow rotation for generalized soil areas mapped in southern Saskatchewan. *Canadian Journal of Soil Science*, *64*, 667−680.

DeFries, R., Hansen, M., Steininger, M., Dubayah, R., Sohlberg, R., & Towshend, J. (1997). Subpixel forest cover in central Africa from multisensor, multitemporal data. *Remote Sensing of Environment*, *60*, 228−246.

Devito, K. J., Hill, A. R., & Roulet, N. T. (1996). Groundwater-surface water interactions in headwater forested wetlands of the Canadian Shield. *Journal of Hydrology*, *181*, 127−147.

Douville, H. (1998). Validation and sensitivity of the global hydrologic budget in stand alone simulations with the ISBA land-surface scheme. *Climate Dynamics*, *14*, 151−171.

Dümenil, H., & Todini, E. (1992). A rainfall-runoff scheme for use in the Hamburg climate model. *Advances in Theoretical Hydrology*, *9*, 129−157.

El Maayar, M., Price, D., Black, T. A., & Humphreys, H. (2002). Sensitivity tests of the integrated biosphere simulator to soil and vegetation characteristics in a pacific coastal coniferous forest. *Atmosphere-Ocean*, *40*(3), 313−332.

Entekhabi, D., & Eagleson, P. S. (1989). Land surface hydrology parameterization for atmospheric general circulation models including subgrid scale spatial variability. *Journal of Climate*, *2*, 816−831.

Essery, R. (2003). Aggregated and distributed modelling of snow cover for a high-latitude basin. *Global and Planetary Change*, *38*, 115−120.

Famiglietti, J. S., & Wood, E. F. (1994). Multi-scale modeling of spatially-variable water and energy balance processes. *Water Resources Research*, *30*, 3061−3078.

Farrar, J. L. (1995). *Trees in Canada*. Fitzhenry and Whiteside Limited and the Canadian Forest Service in cooperation with the Canada Communication Group-publishing, 502 pp.

Fluxnet-Canada (2003). *Fluxnet-Canada annual progress report.* 145 pp.

Gower, S. T., Krankina, O., Olson, R. J., Apps, M., Linder, S., & Wang, C. (2001). Net primary production and carbon allocation patterns of boreal forest ecosystems. *Ecological Applications*, *11*, 1395−1411.

Gower, S. T., Vogel, J. G., Norman, J. M., Kucharik, C. J., Steele, S. J., & Stow, T. K. (1997). Carbon distribution and aboveground net primary production in aspen, jack pine, and black spruce stands in Saskatchewan and Manitoba, Canada. *Journal of Geophysical Research*, *102*(D24), 29,029−29,041.

Grant, R. F. (2004). Modelling topographic effects on net ecosystem productivity of boreal black spruce forest. *Tree Physiology*, *24*, 1−18.

Haddeland, I., Matheussen, B. V., & Lettenmaier, D. P. (2002). Influence of spatial resolution in a macroscale hydrologic model. *Water Resources Research*, *38*(7), 1124−1133.

Hall, F. G., Knapp, D. E., & Huemmrich, K. F. (1997). Physically based classification and satellite mapping of biophysical characteristics in the southern boreal forest. *Journal of Geophysical Research*, *102*, 29,567−29,580.

Jackson, R. B., Canadell, J., & Ehleringer, J. R. (1996). A global analysis of root distributions for terrestrial biomes. *Oecologia*, *108*, 389−411.

Jarvis, P. G. (1976). The interpretation of the variations in leaf water potential and stomatal conductance found in canopies in the field. *Philosophical Transactions of the Royal Society of London, Series B*, *273*, 593−610.

Jarvis, P. G. (1995). Scaling processes and problems. *Plant, Cell & Environment*, *18*, 1079−1089.

Jarvis, P. G., Massheder, J. M., Hale, S. E., Moncrieff, J. B., Rayment, M., & Scott, S. L. (1997). Seasonal variation of carbon dioxide, water vapor, and energy exchanges of a boreal black spruce forest. *Journal of Geophysical Research*, *102*(D24), 28953−28966.

Kang, S., Doh, S., Lee, D., Lee, D., Jin, V. L., & Kimball, J. S. (2003). Topographic and climatic controls on soil respiration in six temperate mixed-hardwood forest slopes, Korea. *Global Change Biology*, *9*, 1427−1437.

Kang, S., Lee, D., & Kimball, J. S. (2004). The effects of spatial aggregation of complex topography on hydroecological process simulations within a rugged forest landscape: Development and application of a satellite-based topoclimatic model. *Canadian Journal of Forest Research*, *34*, 519−530.

Keller, G., & Warrack, B. (1997). *Statistics for managements and economics*, Fourth edition : Duxbury Press. 1073 pp.

Kenward, T., Lettenmaier, D. P., Wood, E. F., & Fielding, E. (2000). Effects of digital elevation model accuracy on hydrologic predictions. *Remote Sensing of Environment*, *74*, 432−444.

Kimball, J. S., Running, S. W., & Saatchi, S. S. (1999). Sensitivity of boreal forest regional water flux and net primary production simulations to sub-grid-scale land cover complexity. *Journal of Geophysical Research*, *104* (D22), 27789−27801.

Kirkby, M. J. (1975). Hydrograph modeling strategies. In R. Peel, M. Chisholm, & P. Haggett (Eds.), *Processes in physical and human geography* (pp. 69−90). London: Heinemann.

Koster, R. D., & Suarez, M. J. (1992). Modelling the land surface boundary in climate models as a composite of independent vegetation stands. *Journal of Geophysical Research*, *97*, 2697−2715.

Liu, J., Chen, J. M., & Cihlar, J. (2003). Mapping evapotranspiration based on remote sensing: An application to Canada's landmass. *Water Resources Research*, *39*(7), 1189.

Mackay, D. S., Ahl, D. E., Ewers, B. E., Gower, S. T., Burrows, S. N., Samanta, S., et al. (2002). Effects of aggregated classifications of forest composition on estimates of evapotranspiration in a northern Wisconsin forest. *Global Change Biology*, *8*, 1252−1265.

Mitchell, S. W., Csillag, F., & Tague, C. (2005). Impacts of spatial partitioning in hydroecological models: Predicting grasslands productivity with RHESSys. *Transactions in GIS*, *9*(3), 423−444.

Nakane, K., Kohno, T., Horikoshi, T., & Nakatsubo, T. (1997). Soil carbon cycling at a black spruce (*Picea mariana*) forest stand in Saskatchewan, Canada. *Journal of Geophysical Research*, *102*(D24), 28785−28793.

Nijssen, B., Haddeland, I., & Lettenmaier, D. P. (1997). Point evaluation of a surface hydrology model for BOREAS. *Journal of Geophysical Research*, *102*, 29,367−29,378.

Nijssen, B., Lettenmaier, D. P., Liang, X., Wetzel, S. W., & Wood, E. F. (1997). Streamflow simulation for continental-scale river basins. *Water Resources Research*, *33*, 711−724.

Patty, E., Desjardins, R. L., & St. Amour, G. (1997). Mass and energy exchanges over a black spruce forest during key periods of BOREAS 1994. *Geophysical Research*, *102*(D24), 28,967−28,975.

Peck, E. L., Carroll, T. R., Maxson, R., Goodison, B., & Metcalfe, J. (1997). Variability of soil moisture near flux towers in the BOREAS southern study area. *Journal of Geophysical Research*, *102*(D24), 28,379−28,388.

Pellenq, J., Kalma, J., Boulet, G., Saulnier, G. -M., Wooldridge, S., Kerr, Y., et al. (2003). A disaggregation scheme for soil moisture based on topography and soil depth. *Journal of Hydrology*, *276*, 112−127.

Pitman, A. J. (1994). Assessing the sensitivity of a Land-Surface-Scheme to the parameter values using a single column model. *Journal of Climate*, *7*, 1856−1869.

Price, D. T., McKenney, D. W., Nalder, I. A., Hutchinson, M. F., & Kesteven, J. L. (2000). A comparison of two statistical methods for spatial interpolation of Canadian monthly mean climate data. *Agricultural and Forest Meteorology*, *101*, 81−94.

Rastetter, E. B., Aber, J. D., Peters, D. P. C., Ojima, D. S., & Burke, I. (2003). Using mechanistic models to scale ecological processes across space and time. *Bioscience*, *53*, 68−76.

Rastetter, E. B., King, A. W., Cosby, B. J., Hornberger, G. M., O'Neill, R. V., & Hobbie, J. E. (1992). Aggregating fine-scale ecological knowledge to model coarser-scale attributes of ecosystems. *Ecological Applications*, *2*, 55−70.

Running, S. W., Thornton, P. E., Nemani, R. R., & Glassy, J. M. (2000). Global terrestrial gross and net primary productivity form the Earth observing system. In O. Sala, R. Jackson, & H. Mooney (Eds.), *Methods in ecosystem science* New York: Springer-Verlag.

Seth, A., Giorgi, F., & Dickinson, R. E. (1994). Simulating fluxes from heterogeneous land surfaces: explicit subgrid method employing the biosphere-atmosphere transfer scheme (BATS). *Journal of Geophysical Research*, *99*, 651−677.

Simic, A., Chen, J. M., Liu, J., & Csillag, F. (2004). Spatial scaling of net primary productivity using subpixel information. *Remote Sensing of Environment*, *93*, 246−258.

Steyaert, L. T., Hall, F. G., & Loveland, T. R. (1997). Land cover mapping, fire regeneration, and scaling studies in the Canadian boreal forest with 1 km AVHRR and Landsat TM data. *Journal of Geophysical Research*, *102*, 29581−29598.

Storck, P., Bowling, L., Wetherbee, P., & Lettenmaier, D. (1998). Application of a GIS-based distributed hydrology model for prediction of forest harvest effects on peak stream flow in the Pacific Northwest. *Hydrological Processes*, *12*, 889−904.

Storck, P., Bowling, L., Wetherbee, P., & Lettenmaier, D. (1999). Application of a GIS-based distributed hydrology model for prediction of forest harvest effects on peak stream flow in the Pacific Northwest. In A. M. Gurnell, & D. R. Montgomery (Eds.), *Hydrological applications of GIS* : John Wiley and Sons.

Strayer, D. L., Holly, A. E., & Bigelow, S. (2003). What kind of spatial and temporal details are required in models of heterogenous systems? *Oikos*, *102*, 654−662.

Turner, D. P., Dobson, R., & Marks, D. (1996). Comparison of alternative spatial resolutions in the application of a spatially distributed bio-geochemical model over complex terrain. *Ecological Modelling*, *90*(1), 53−67.

VanShaar, J. R., Haddeland, I., & Lettenmaier, D. P. (2002). Effects of land cover changes on the hydrologic response of interior Columbia River Basin forested catchments. *Hydrological Processes*, *16*, 2499−2520.

Verseghy, D. L., McFarlane, N. A., & Lazare, M. (1993). CLASS-A Canadian land surface scheme for GCMs, II, vegetation model and coupled runs. *International Journal of Climatology*, *13*, 347−370.

Verstrate, M. M., Pinty, B., & Myneni, R. B. (1996). Potential and limitations of information extraction on the terrestrial biosphere from satellite remote sensing. *Remote Sensing of Environment*, *58*, 201−214.

Walko, R. L., Band, L. E., Baron, J., Kittel, T. G. F., Lammers, R., Lee, T. J., et al. (2000). Coupled atmosphere-biophysics-hydrology models for environmental modeling. *Journal of Applied Meteorology*, *39*, 931−944.

Walland, D. J., & Simmonds, I. (1996). Subgrid-scale topography and the simulation of Northern Hemisphere snow cover. *International Journal of Climatology*, *16*, 961−982.

Wetzel, P. J., & Chang, J. -T. (1988). Evapotranspiration from nonuniform surfaces: Afirst approach for short-term numerical weather predictions. *Monthly Weather Review*, *116*, 600−621.

Whitaker, A., Alila, Y., Beckers, J., & Toews, D. (2003). Application of the distributed hydrology soil vegetation model to redfish creek, British Columbia: Model evaluation using internal catchment data. *Hydrological Processes*, *17*, 199−224.

Wigmosta, M. S., Vail, L. W., & Lettenmaier, D. P. (1994). A distributed hydrology-vegetation model for complex terrain. *Water Resources Research*, *30*(6), 1665−1679.

Wood, E.F. (1997). Effect of soil moisture aggregation on surface evaporative fluxes. 190, 397–412.

Wood, E. F., Lettenmaier, D. P., & Zartanian, V. (1992). A land surface hydrology parameterization with sub-grid variability for general circulation models. *Journal of Geophysical Research*, *97*(D3), 2717−2728.

Zeng, D., Hunt Jr., E. R., & Running, S. W. (1996). Comparison of available soil water capacity estimated from topography and soil series information. *Landscape Ecology*, *11*, 3−14.